

VILNIUS UNIVERSITY  
CENTER FOR PHYSICAL SCIENCES AND  
TECHNOLOGY

JUSTINAS GALINIS

**RESEARCH ON SPONTANEOUS  
PARAMETRIC DOWN-CONVERSION  
PUMPED BY INCOHERENT LIGHT  
SOURCES**

*Summary of doctoral dissertation*

*Physical sciences, Physics (02P)*

Vilnius, 2014

The doctoral dissertation was prepared during 2010 – 2014 in Vilnius University.

**Scientific supervisor:**

dr. Gintaras Tamošauskas (Vilnius University, Physical sciences, Physics - 02P).

**Doctoral committee:**

**Chairman** – prof. Roaldas Gadonas (Vilnius University, Physical sciences, Physics - 02P).

**Members:**

habil. dr. Gediminas Juzeliūnas (Vilnius University, Institute of Theoretical Physics and Astronomy, Physical sciences, Physics - 02P)

dr. Vygantas Jarutis (Vilnius University, Physical sciences, Physics - 02P)

dr. Ramūnas Adomavičius (Center for Physical Sciences and Technology, Physical sciences, Physics - 02P)

dr. Martynas Beresna (Southampton University, Optoelectronics Research Center (United Kingdom), Physical sciences, Physics - 02P)

The dissertation will be defended under open consideration in the Council of Physics on the 12th September, 2014, 14h at the Laser Research Center of Vilnius University, room 306.

Address: Saulėtekio av. 10, Vilnius, Lithuania.

The summary of the dissertation was distributed on the 12th August, 2014.

The dissertation is available at Vilnius University and Center for Physical Sciences and Technology libraries.

VILNIAUS UNIVERSITETAS  
FIZINIŲ IR TECHNOLOGIJOS MOKSLŲ  
CENTRAS

JUSTINAS GALINIS

**PARAMETRINĖS FLUORESCENCIJOS  
ŽADINAMOS NEKOHERETINIAIS  
ŠVIESOS ŠALTINIAIS TYRIMAS**

*Daktaro disertacija*  
*Fiziniai mokslai, Fizika (02P)*

Vilnius, 2014 metai

Disertacija rengta 2010 – 2014 metais Vilniaus universitete

**Mokslinis vadovas:**

dr. Gintaras Tamošauskas (Vilniaus universitetas, fiziniai mokslai, fizika - 02P).

**Disertacija ginama Vilniaus universiteto Fizikos mokslo krypties taryboje:**

**Pirmininkas** – prof. Roaldas Gadonas (Vilniaus universitetas, fiziniai mokslai, fizika - 02P).

**Nariai:**

habil. dr. Gediminas Juzeliūnas (Vilniaus universitetas, Teorinės fizikos ir astronomijos institutas, fiziniai mokslai, fizika - 02P)

dr. Vygantas Jarutis (Vilniaus universitetas, fiziniai mokslai, fizika - 02P)

dr. Ramūnas Adomavičius (Fizinių ir Technologijos mokslų centras, fiziniai mokslai, fizika - 02P)

dr. Martynas Beresna (Southampton universitetas, Optoelektronikos tyrimų centras (Didžioji Britanija), fiziniai mokslai, fizika - 02P)

Disertacija bus ginama viešame Fizikos mokslo krypties tarybos posėdyje 2014 m. rugsėjo mėn. 12 d. 14 val. Vilniaus Universiteto Lazerinių Tyrimų Centre 306 auditorijoje.

Adresas: Saulėtekio al. 10, Vilnius, Lietuva.

Disertacijos santrauka išsiuntinėta 2014 m. rugpjūčio mėn. 12 d.

Disertaciją galima peržiūrėti Vilniaus universiteto ir Fizinių ir technologijos mokslų centro bibliotekose.

# Contents

List of the abbreviations . . . . .	3
<b>Introduction</b>	<b>4</b>
<b>1 Nature of spontaneous parametric down-conversion</b>	<b>11</b>
<b>2 Research on SPDC pumped with a high-power blue LED</b>	<b>14</b>
2.1 Experimental setup . . . . .	14
2.2 Angular distributions of SPDC . . . . .	16
2.3 Power analysis of type I SPDC . . . . .	17
2.4 Summary . . . . .	18
<b>3 Simulation of SPDC pumped by a high power LED</b>	<b>19</b>
3.1 Theoretical model of SPDC excited by incoherent light sources . . . . .	19
3.2 Theoretical characterization of the experimental SPDC power distribution . . . . .	20
3.3 Summary . . . . .	23
<b>4 Statistical analysis of a biphoton field excited by a blue LED</b>	<b>24</b>
4.1 Experimental setup . . . . .	24
4.2 Research on the biphoton statistical distribution . . . . .	25
4.3 Summary . . . . .	26
<b>5 Research on SPDC excited by a blue LED in LiIO<sub>3</sub> crystal photon coincidences</b>	<b>27</b>
5.1 Principles of photon coincidence measurements . . . . .	27
5.2 Experimental setup . . . . .	28
5.3 Coincidence results for twin photons pumped by different parameter pump beams . . . . .	29
5.4 Summary . . . . .	31
<b>6 Theoretical analysis of a biphoton field excited by incoherent radiation</b>	<b>32</b>
6.1 Theoretical model of the SPDC photon coincidences . . . . .	32
6.1.1 Geometric factor . . . . .	34
6.2 Theoretical simulation of a broadband biphoton field excited in dispersive media . . . . .	35
6.3 Theoretical simulation of experimental photon coincidence results . . . . .	37

6.4 Summary . . . . .	39
<b>Conclusions</b>	<b>40</b>
<b>Bibliography</b>	<b>42</b>
<b>Santrauka</b>	<b>46</b>
<b>Curriculum vitae</b>	<b>47</b>

## List of abbreviations

BBO -  $\beta BaB_2O_4$  - beta barium borate  
CCD - Charge-Coupled Device  
*e* polarization - extraordinary polarization  
FWHM - Full Width at Half Maximum  
KDP -  $KH_2PO_4$  - potassium dihydrophosphate  
LED - Light-Emitting Diode  
NA - Numerical Aperture  
SPDC - Spontaneous Parametric Down-Conversion  
*o* polarization - ordinary polarization  
TTL - Transistor–Transistor Logic electrical impulse

# Introduction

The 20th century was especially rich in scientific discoveries. One of the most prominent and the most important scientific works - the laser - widely opened the door to new areas of research. The laser has become an integral tool in various scientific laboratories where the properties of light and light interaction with materials is explored. For the first few years of its existence, the laser has been studied on a wide variety of optical phenomena that occur in ultra-intense light field interaction with materials - the second harmonic generation, optical parametric oscillation or parametric amplification [1]. During theoretical research on the optical parametric amplifier noise, spontaneous parametric down conversion (SPDC) was discovered [2, 3]. Several years passed, and theoretical considerations have been realized experimentally in the  $\text{LiNbO}_3$  crystal using an argon laser [4, 5]. Over time, research on SPDC increased and the scientific community firmly established the tradition of pumping SPDC with laser radiation.

SPDC could be called the pump photon scatter, because the pump photon splits into two parametric photons of lower frequency due to energy and momentum conservation laws. Parametric twin photons under the agreement are called the signal (higher frequency) and idler (lower frequency) photons. This parametric radiation can also be called a biphoton field, because it consists of a pair of photons born from individual pump photons. The biphoton field has a characteristic spatial photon distribution cone due to the quadratic nonlinearity of nonlinear, media dispersion and phase-matching conditions. A special biphoton field case is entangled photons, photons which are concerned to each another in energy, polarization and propagation direction. Entangled photons are widely used in a wide spectrum of quantum optics experiments [6–12]. For this reason, one of the main applications of the SPDC is entangled photon generation [13].

Although SPDC is usually excited by laser radiation, experimental examples can be found in the scientific literature, where SPDC is generated using spatially incoherent radiation - a mercury lamp spectral line [15]. On the other hand, there have been no scientific studies to determine whether a biphoton field can be excited using both spatially and temporally incoherent radiation. It is well known that SPDC power directly depends on the pumping power but not on the intensity when parametric amplification does not occur [1]. This raises the question as to whether it is possible to register SPDC, pumped by simple LED radiation, and what kind of features such a biphoton field will have.

**The main aim of this thesis** was experimentally to investigate the ability to generate an SPDC pumping by both temporal and spatially incoherent radiation



- a high-power blue LED. In addition, it aimed to determine the influence of the spatial and spectral composition of the pump radiation field on the biphoton field properties, investigate the opportunities for changing biphoton field structure, to explore the possibilities of applying a biphoton field pumped by the blue LED in quantum optics experiments.

## Tasks

During the thesis preparation period the following tasks were completed:

1. Research on incoherent source application for SPDC excitation in various nonlinear crystals (KDP, LiIO<sub>3</sub>, BBO). Research on SPDC spatial distribution dependence on pump beam spatial and frequency spectral characteristics.
2. Development of the SPDC simulation program. Theoretical analysis of experimental data in order to explain both the spatial and spectral characteristics of the PF beam.
3. Research on the statistical properties of the biphoton field when excited with an incoherent light source. Analysis of detectors afterpulse generation influence on the statistical distribution of the biphoton field.
4. Experimental research on biphoton field photon coincidences using an incoherent pump source. Research of pump beam spatial and spectral characteristics, detection spatial and spectral characteristics and orientation of nonlinear crystal influence on biphoton field singles and coincidences both quantitative and qualitative properties.
5. Development of photon coincidences simulation program.
6. Theoretical research on the perspectives of incoherent source application for the excitation of a qualitative biphoton field
7. Theoretical research on biphoton field pumped with an incoherent light source in dispersive medium quantitative parameters using both limited and unlimited detection channel apertures.
8. Theoretical analysis of experimental photon coincidences data in order to quantitatively explain the spectral and spatial properties of single photons and photon coincidences.

## Novelty

1. The generation of SPDC pumped with incoherent radiation - high-power blue LED was experimentally demonstrated in large aperture nonlinear media for the first time. It was experimentally demonstrated that it is possible to register a weak SPDC signal using high sensitivity modern detectors.

2. The influence of pump beam spatial and spectral characteristics on spatial distribution of the SPDC power was theoretically investigated for the first time. The original theoretical simulation program allows for both qualitatively and quantitatively describing the spatial and spectral properties of the biphoton field pumped with incoherent radiation. Using the numerical simulation results, it is possible to determine the optimal experimental conditions for the excitation of the desired SPDC field spectral characteristics.
3. A statistical analysis of a biphoton field pumped with incoherent radiation was performed. It was found to be impossible to describe the quality of broadband light field statistical properties using experimental conditions. A negative binomial distribution mode parameter was proposed, which describes the spatial and spectral modes number of the emitted light field. Some modifications of the experimental conditions were suggested, which would enable one to perform a correct statistical analysis of the broadband biphoton field.
4. Biphoton field pumped with an incoherent radiation photon coincidence measurements were experimentally demonstrated for the first time. These measurements allow us to qualitatively describe the biphoton field and define its suitability for quantum optics experiments. Sufficiently large experimentally recorded photon coincidences and the average relative coincidences suggest that incoherent radiation can be applied for the quantum optics experiments as an average quality biphoton field pump source.
5. Theoretically investigated the perspectives of broadband incoherent radiation for the biphoton field excitation. Theoretically determined spatial and spectral pump field characteristics influence on the properties of photon coincidences. It was found that biphoton fields pumped with broadband incoherent radiation are qualitatively similar to a biphoton field pumped with broadband laser radiation. The theoretical modeling program allows us to determine the optimal spatial and spectral parameters of a detection channel for high-quality photon coincidence generation.

## Practical value

The main practical value of the research is that it was experimentally revealed that incoherent sources are appropriate for biphoton field generation and application to quantum optics experiments. It is obvious that coherent laser radiation can excite the best spatial characteristics biphoton field with an extremely high biphoton flux due to the high irradiance of laser radiation. On the other hand incoherent sources could be an excellent alternative to laser systems for medium quality biphoton flux applications. The main advantages of the incoherent sources are low cost, simple production technology and the huge commercial variety of different wavelength sources. One of the most important application of biphoton fields pumped with incoherent radiation could be quantum tomography. In this case, a small coherent biphoton field has a great advantage, because it leads to high resolution in quantum tomography.

The simulation program developed for the SPDC power distributions allows one to choose the optimal pump beam, SPDC generation and detection conditions, and to be able to generate a biphoton field with the desired spectral and spatial properties. The simulation program also allows one to evaluate the quality of the biphoton field for selected initial conditions.

## Statements to defend

1. Both temporally and spatially incoherent radiation can be used for SPDC excitation. Modern CCD cameras can be used for the detection of SPDC radiation excited with the incoherent sources which spectral irradiance is significantly lower than the solar spectral irradiance. Generated SPDC power is directly proportional to the incoherent pump power.
2. The power spatial distribution of an SPDC, pumped with the incoherent sources depends on the nonlinear media dispersion properties and the spatial and spectral composition of the pump radiation. KDP crystal dispersion properties determine that the SPDC power distribution essentially depends only on the pump spectrum - for the wider spectrum asymmetry of the SPDC power distribution is more visible. In  $\text{LiIO}_3$  crystal case SPDC power distribution essentially depend on the spatial spectrum of the pump - wider spatial spectrum of the pump determines wider SPDC spatial distribution.
3. A biphoton field pumped with incoherent radiation in  $\text{LiIO}_3$  crystal has quite large coincidences flow and relative coincidence number. These parameters directly depend on the number of pump components involved in the nonlinear interaction: the maximum photon coincidences flux is achieved with the highest pump power, the relative coincidence number is highest for the smallest diameter and divergence of the pump beam.
4. A biphoton field pumped with broadband incoherent radiation has high quality, equivalent to a biphoton field pumped with laser radiation. Photon coincidence results can be evaluated both qualitatively as well as quantitatively using the theoretical model of SPDC excited with both spatially and temporally incoherent radiation.

## Approbation

### Scientific papers related to the thesis topics

- A1 G. Tamošauskas, **J. Galinis**, A. Dubietis, and A. Piskarskas, Observation of spontaneous parametric down-conversion excited by high brightness blue LED, *Opt. Express* **18**, 4310-4315 (2010).
- A2 **J. Galinis**, M. Karpiński, G. Tamošauskas, K. Dobek, and A. Piskarskas, Photon coincidences in spontaneous parametric down-converted radiation excited by a blue LED in bulk  $\text{LiIO}_3$  crystal, *Optics Express* **19**, 10351-10358 (2011).

- A3 **J. Galinis**, G. Tamošauskas, and A. Piskarskas, Modeling of photon coincidence and dispersive properties of spontaneous parametric down-converted field excited by incoherent source, *Opt. Commun.* **285**, 1289-1296 (2012).
- A4 **J. Galinis**, M. Karpiński, G. Tamošauskas, K. Dobek, and A. Piskarskas, Photon correlation and statistics of spontaneous parametric down conversion pumped by blue LED in LiIO<sub>3</sub> crystal, *Lith. J. Phys.* **52**, 285–294 (2012).

### Conference presentations

- **J. Galinis**, Parametrinės fluorescencijos, žadinamos Saulės spinduliuote, tyrimas, Oral presentation, Conference of PhD students internships in foreign research centers in 2012 – 2013 konferencija, Vilnius, October 11, 2013.
- **J. Galinis**, G. Tamošauskas, V. Jukna, and A. Dubietis, Femtosekundinio šviesos superkontinuumo plėtra ilgųjų bangų srityje, Abstr. of 40th Lithuanian National Physicists Conference, Vilnius, June 10-12, 2013.
- **J. Galinis**, M. Karpiński, G. Tamošauskas, K. Dobek, and A. Piskarskas, Photon coincidences in spontaneous parametric down-converted radiation excited by a blue LED in LiIO<sub>3</sub> crystal, Abstr. of 500. WE-Heraeus Seminar Highlights of Quantum Optics, Bad Honnef (Germany), May 7-11, 2012.
- **J. Galinis**, Dvyninio lauko, žadinamo mėlynu šviesos diodu LiIO<sub>3</sub> ir BBO kristaluose, kvantinių būsenų valdymas, Abstr. And Oral presentation of Second Conference of Young Scientists, Vilnius, February 14, 2012.
- **J. Galinis**, M. Karpiński, G. Tamošauskas, K. Dobek, and A. Piskarskas, Photon coincidences and statistics in spontaneous parametric down-converted radiation excited by a blue LED in LiIO<sub>3</sub> crystal, Abstr. of 39th Lithuanian National Physicists Conference, Vilnius, October 6-8, 2011.
- **J. Galinis**, Observation of spontaneous parametric down-conversion excited by high-brightness blue LED, Abstr. of Alexander von Humboldt Forum "Science & Society in Modern Europe" Dedicated to Millennium of Lithuania and 50 Years of the Laser, Vilnius (Lithuania), September 23-26 2010.
- G. Tamošauskas, **J. Galinis**, A. Dubietis, and A. Piskarskas, Observation of spontaneous parametric down-conversion excited by high-brightness blue LED, Abstr. and Oral presentation at the Advanced Photonics 2010 - Nonlinear Photonics Topical Meeting, Karlsruhe (Germany), NThC5, June 21-24 2010.
- **J. Galinis**, Observation of spontaneous parametric down-conversion excited by high-brightness blue LED, Abstr. of 53th scientific conference for young students of physics and natural sciences Open Readings, Vilnius, 24-27 March 2010, page 144.
- G. Tamošauskas, **J. Galinis**, A. Dubietis, and A. Piskarskas, Observation of spontaneous parametric down-conversion excited by high-brightness blue LED,

Abstr. of 453. WE-Heraeus Seminar Quantum Communication based on Integrated Optics, Bad Honnef (Germany), 22-25 March 2010.

### Other scientific papers

- V. Jukna, **J. Galinis**, G. Tamošauskas, D. Majus, and A. Dubietis, Infrared extension of femtosecond supercontinuum generated by filamentation in solid-state media, Applied Physics B: Lasers and Optics, DOI: 10.1007/s00340-013-5723-8 (2013).
- F. Sciarrino, G. Vallone, G. Milani, A. Avella, **J. Galinis**, R. Machulka, A. M. Perego, K. Y. Spasibko, A. Allevi, M. Bondani, and P. Mataloni, High degree of entanglement and nonlocality of a two-photon state generated at 532 nm, European Physical Journal Special Topics, **199**, 111-125 (2011).
- H. Valtna, A. Dubietis, G. Tamošauskas, P. Polesana, **J. Galinis**, D. Majus, D. Faccio, P. Di Trapani, and A. Piskarskas, Efficient four-wave parametric amplification and spatial soliton generation on transparent isotropic medium with Kerr nonlinearity, Lith. J. Phys., **47**, 403-410 (2007).

### Contributions

Most of the experiments described in this thesis were performed in Vilnius University, Department of Quantum Electronics in 2010 – 2014 under the supervision of Dr. Gintaras Tamošauskas. Part of the experiments were performed in Toruń (Poland), Nicolaus Copernicus University in Institute of Physics during the internship visit with Polish colleagues Dr. Michael Karpiński and Dr. Krzysztof Dobek. All the theoretical simulations described in this dissertation were performed by the author himself, all the experiments were performed in collaboration with coworkers. Therefore it is important to distinguish the contribution from these co-authors:

- **prof. A. P. Piskarskas** created an idea to pump SPDC with incoherent sources, initiated the research, advised on scientific issues in the research, initiated conditions for the research, travel to scientific internship in Poland and presentation of the research results to the wide scientific community.
- **prof. A. Dubietis** consulted on various scientific topics during the research, meaningfully contributed to [A1] paper writing.
- **dr. G. Tamošauskas** supervised all research progress, was one of the main co-worker performing the experiments, consulted performing the theoretical simulation, interpreting the data and creating new research topics. He also meaningfully contributed to writing papers, consulted in data preparation for presentation in various conferences and seminars.
- **dr. M. Karpiński** was one of the co-workers preparing photon coincidences experiments in Toruń, consulted about the topics of photon coincidences and photon statistics, consulted about the data analysis and interpretations, contributed to [A2] paper writing.

- **dr. K. Dobek** was one of the co-workers preparing photon coincidences experiments in Toruń.

Discussions with *prof. A. Stabinis*, *Dr. V. Jukna* were useful for theoretical simulations. *Dr. V. Jarutis*, *prof. M. Bondani* consulted about quantum optics topics.

## Structure of the thesis

The thesis is divided into six main chapters. The first chapter provides the SPDC introduction, explains the nature of this phenomenon and the spatial features of the semi-classical description of the SPDC. In the second chapter experimental SPDC pumped with high-power blue LED results are presented. The experimental scheme and SPDC power distributions in three different nonlinear crystals are presented. In the third chapter theoretical analysis of SPDC pumped with a high-power blue LED is described. The numerical simulation program for SPDC power distribution is described; the causes of the spatial distribution of SPDC are analyzed. In the fourth chapter, the experimental biphoton field statistical analysis is presented. Various light fields statistical studies in the scientific literature are overviewed, the experimental setup is described, the biphoton field is characterized using the negative binomial distribution and the influence of detectors afterpulses generation probability on the statistical results is discussed. In the fifth chapter, the experimental results of photon coincidences are described. An overview of quantum optics research related to the entangled states in the scientific literature is presented, the photon coincidences registration method is overviewed, the experimental scheme and experimental results of photon coincidences pumped with different diameter and divergence pump beam are presented. In Chapter Six, theoretical results of biphoton field photon coincidence are presented. The numerical simulation program for photon coincidences theoretical analysis is presented, theoretical perspectives of broadband incoherent light usage for the excitation of the biphoton field is evaluated and the experimental data presented in Chapter 5 are analyzed. The conclusions and references are presented at the end of the dissertation.

# 1

## Nature of spontaneous parametric down-conversion

Spontaneous parametric down-conversion (SPDC) is a nonlinear process in which pump wave scattering appears due to the quantized field fluctuations in the quadratic nonlinear materials. The high-frequency pump wave splits into two lower frequency parametric waves. The parametric wave frequency and direction is determined by energy and momentum conservation laws. The energy conservation law defines that the sum of generated parametric wave frequencies must be equal to the pump frequency ( $\omega_p = \Omega_s + \omega_i$ ). Under an agreement the higher frequency parametric wave is called a signal, lower frequency – an idler. The momentum conservation law ( $k_p = k_s + k_i$ ,  $k$  - wave number, Fig. 1.1), also known as phase matching, determines the directions in which the parametric waves will propagate. These couples of waves are also called biphotons or photon twins, because they were born from the same individual pump photon at the same time. Biphotons are unique because they are related to each another by the frequency, propagation direction and polarization [16]. In short, SPDC can be thought of as a non-coherent light scatter, during which real material excitation does not exist [1].

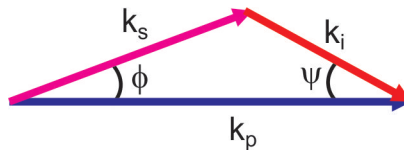


**Figure 1.1:** SPDC phase matching; here  $k_p$  - pump wavenumber  $k_s$  - signal wavenumber  $k_i$  - idler wavenumber,  $\phi$  - angle between signal and pump waves,  $\psi$  - angle between idler and pump waves.

Two types of nonlinear interactions can be excited in the negative uniaxial crystals. In the type I interaction (e - oo) one extraordinary (e) polarization of the pump photon mixing with the ordinary (o) polarized idler photon creates an ordinary polarized signal photon. In the type II interaction (e - eo) the e polarized pump photon splits into two different polarized photons: e signal and o idler photons and vice versa. Under the agreement, o polarized waves are those waves for which the electric field vector oscillates perpendicularly to the optical axis of the crystal, while e polarization waves - in parallel. The SPDC field is cone shaped in the negative

uniaxial crystals, because the probability of creating parametric wave pairs in all phase-matching directions is the same. During the Type I nonlinear interaction, polarization of the signal and idler waves is the same, therefore the integral SPDC light field is a uniform cone symmetrically located around the pump wave (Fig. 1.2 (a)).

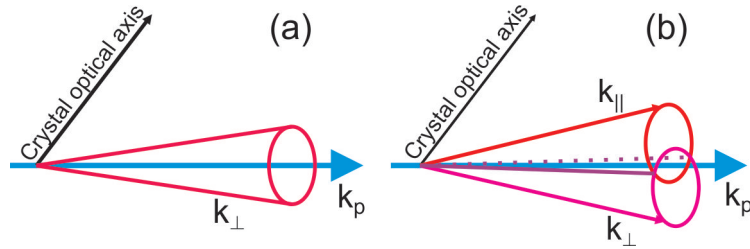


**Figure 1.2:** SPDC field cones spatial location during Type I (a) and Type II (b) nonlinear interaction in negative uniaxial crystals;  $k_p$  - pump wavenumber,  $k_{\perp}$  - orthogonal (*o*) polarization wavenumber  $k_{\parallel}$  - parallel (*e*) polarization wavenumber.

In Type II parametric interaction, different polarization (*o* and *e*) parametric waves are created. Extraordinary polarized waves are characterized by the fact that their phase velocity (also the refractive index) in nonlinear media depends on the propagation direction in the media (deviation angle  $\phi$  from the crystal optical axis). The light wavenumber is inversely proportional to the phase velocity of light  $v_f$ :  $k = \frac{\omega}{v_f} = \frac{n\omega}{c}$ , here  $n$  - refraction index,  $\omega$  - frequency,  $c$  - speed of light in a vacuum. In other words, the extraordinary polarized light wave number decreases with the increasing angle of  $\phi$ . Due to the geometric features of the phase-matching conditions the type II SPDC beam consists of two different polarization (*e* and *o*) light cones, whose axes do not coincide with the pumping wave (Fig. 1.2 (b)) and are mutually separated by the walk-off angle  $\gamma$ . These type II PF spatial characteristics are unique in that entangled photon states are created along the intersection axes of both cones. These entangled states are one of the most important quantum optics research objects [13].

Let us consider the theoretical model of the SPDC power output in a nonlinear crystal pumped by a monochromatic plane pump wave. In this thesis a semi-classical model is applied calculating SPDC power. The result of the semi-classical model fully coincides with the result of the quantum theory. The mathematical model of the SPDC will be explored using the simpler Type I (*e-oo*) parametric interaction in nonlinear crystals [5]. In this case, the nonlinear crystal is pumped by *e* polarization pump waves and *o* polarization signal and idler wave couples are created, making  $\phi$  and  $\psi$  angles with the pump wave respectively (Fig. 1.1). There is always some probability that the pump wave will split into the signal and idler waves in the case of a weak pump when no parametric amplification appears.

During the nonlinear interaction all the participating waves mix with each other due to the nonlinear polarizability [5]. Signal and idler waves are generated by the pump wave mixing with the quantum noise. In this case it is assumed that pump beam depletion does not occur (parametric power conversion reaches about  $10^{-6}$ ), and that the created signal and idler waves are too weak to create an interaction with the other waves involved in the process. The total power of the SPDC process  $P_s$  is calculated:



$$P_s = L^2 P_p \int_0^\infty \int_{-\pi/2}^{\pi/2} \int_{-\pi/2}^{\pi/2} \frac{\omega_s^4 \omega_i d_{ef}^2 \hbar n_s}{4\pi^3 \varepsilon_0 c^5 n_i n_p} \text{sinc}^2 \frac{\Delta k L}{2} d\varphi d\theta d\omega_s. \quad (1.1)$$

here  $L$  – length of the nonlinear medium,  $P_p$  – pump power,  $\omega_s$  – signal frequency,  $\omega_i$  – idler frequency,  $d_{ef}$  – effective nonlinear coefficient,  $\hbar$  – reduced Planck constant,  $n_s$  – signal wave refraction index,  $\varepsilon_0$  – electric constant,  $c$  – speed of light,  $n_i$  – idler wave refraction index,  $n_p$  – pump wave refraction index,  $\Delta k$  – phase mismatching which is equal to the variance of all wavenumbers participating in the process along the pump wave direction:

$$\Delta k = k_p - k_i \cos \phi - k_s \cos \psi; \quad (1.2)$$

here  $\phi$  – angle between pump and idler waves,  $\varphi$  – angle between pump and signal waves (Fig. 1.1). Parametric interaction is the most effective when phase mismatch is equal to zero.

It is not possible to write down a general analytical expression for the (1.1) formula, therefore SPDC power is calculated using numerical simulations. On the other hand, using certain simplifications for the small detection angles and narrow signal wave spectra we can evaluate the general SPDC power tendencies:

$$P_s = \frac{\beta L P_p}{b} \pi \theta^2; \quad (1.3)$$

here  $\beta$  – parametric conversion constant,  $b = \frac{\partial k_s}{\partial \omega_s} - \frac{\partial k_i}{\partial \omega_i}$  – frequency dispersive constant [17]. Invoking the (1.3) formula it can be concluded that SPDC power is proportional to the signal spatial angle  $\pi \theta^2$ , pump power and nonlinear interaction length.

## 2

# Research on SPDC pumped with a high-power blue LED

*Material related with this chapter was published in paper [A1]*

SPDC was experimentally observed and studied for the first time [4, 5, 18] 7 years after the first laser demonstration in 1960. With the development of light sources, detectors and other optical technologies, this phenomenon quite quickly began to be used as a biphoton source [13, 14, 19] in quantum optics experiments [6–12]. SPDC is also applied in detector quantum efficiency [20] and nonlinear crystals second-order nonlinearity coefficients [21, 22] measurements. The tradition of pumping SPDC with laser radiation was established from the early experiments. As far as is known, only one researcher, D. L. Weinberg, applied the spatially incoherent radiation, mercury lamp single spectral line, for SPDC excitation [15]. However, both temporally and spatially incoherent sources for SPDC excitation were not used. (1.3) formula shows that this phenomenon depends only on the pump beam power, and not on its intensity, and it is not necessary to use high-intensity laser radiation for efficient SPDC generation. On the other hand, SPDC pumped with a laser has much higher irradiance, which is a big advantage for practical applications; therefore lasers completely dominant as pump sources. With the development of high power and low cost light sources, such as LEDs operating in the blue - green spectral range [23], it became possible to use both temporally and spatially incoherent light sources as pump sources in nonlinear optical studies.

In this chapter the first experimental results of SPDC pumped with high-power blue LED in different nonlinear crystals are presented.

## 2.1 Experimental setup

The experimental setup is schematically depicted in Fig. 2.1. The whole setup is assembled in a single black box and consists of three compartments isolated by the optical filters. The first section is dedicated to the pump beam formation, second - nonlinear interaction, third - detection. As a pump source a high-brightness blue

LED is used, emitting 2,5 W power radiation, whose central wavelength is 457 nm, spectral width (FWHM) - 24 nm (Fig. 2.2 (a)). A Glan prism linearly polarizes the LED radiation. The pump beam is shaped with a set of lenses (L1 = +22 mm and L2 = +200 mm) and apertures (D1 and D2). Maximum pump beam power is 0,53 mW The color glass filter F1 is used to block the long-wave radiation (>560 nm).

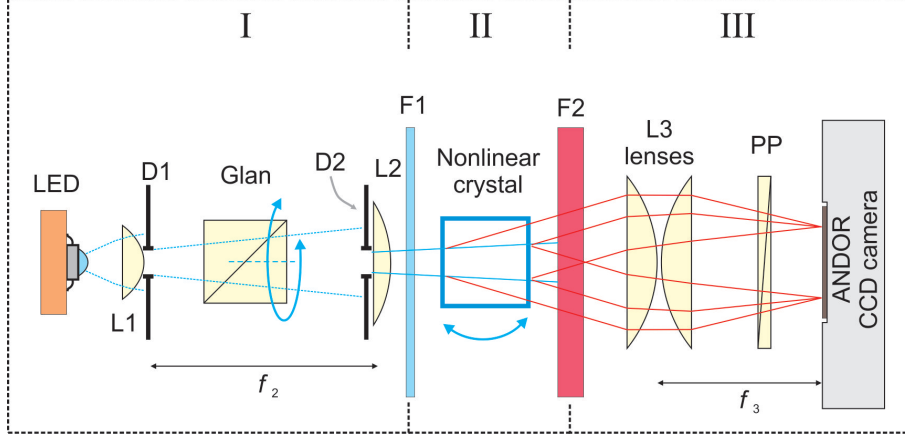


**Figure 2.1:** SPDC pumped with the high-power blue LED experimental setup; D1 and D2 - apertures, L1, L2, L3 - lenses, Glan – Glan prism, F1 – filter blocking the long-wave radiation, F2 – filter blocking the short-wave radiation, PP - the film polarizer,  $f_2$  - L2 lens focal length,  $f_3$  - L3 lens focal length.

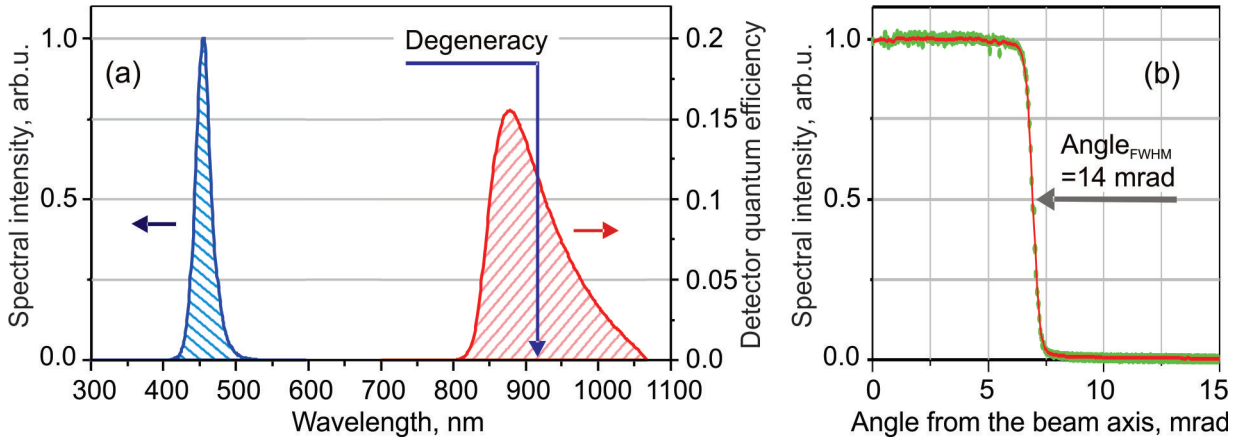


**Figure 2.2:** a) Emission spectrum of the LED and detection system quantum efficiency; (b) Typical pump beam spatial spectrum.

The second section consists of the nonlinear crystal which is mounted on a motorized rotation stage, with rotation in the phase matching  $\theta$  plane. We used three different nonlinear media: 20 mm thick KDP and LiIO<sub>3</sub> crystals, both cut for type I phase matching, and 8 mm thick BBO cut for type II phase matching. Filter F2 is used to absorb visible and some part of infrared radiation (<850 nm), blocking the pump beam from the detection system.

The third section consists of high dynamic range (16 bits) CCD camera (ANDOR DV420A-OE), thermoelectrically cooled down to -50°C. SPDC radiation is collected into the CCD camera using L3 composite lens, whose focal length is  $f_3=+54,6$  mm. The CCD camera is placed in the focus of the L3 lens. In this way, an angular distribution pattern of SPDC is formed on the plane of the CCD sensor. The film

polarizer PP is used to analyze the polarization of the SPDC. The entire detection system quantum efficiency spectrum around the degeneracy ( $\lambda=914$  nm), is illustrated in Fig. 2.2 (a). Detection quantum efficiency is obtained combining the data of the filter transmittance and the quantum efficiency of the CCD camera provided by the manufacturer.

## 2.2 Angular distributions of SPDC

It is known from theory that SPDC radiation has a cone shape. If the image of the central part of the nonlinear crystal is formed on the CCD matrix plane, it is possible to register the spatial distribution of SPDC. Spatial distribution of cone radiation is a ring shape which means that all SPDC components diverge from the pump beam with the same angle in all directions. By rotating the nonlinear crystal in the higher angle direction, it was experimentally observed how SPDC radiation appeared to be axial and later transformed into conical radiation. By increasing the crystal orientation angles, it was observed how the angle of conical radiation increases.

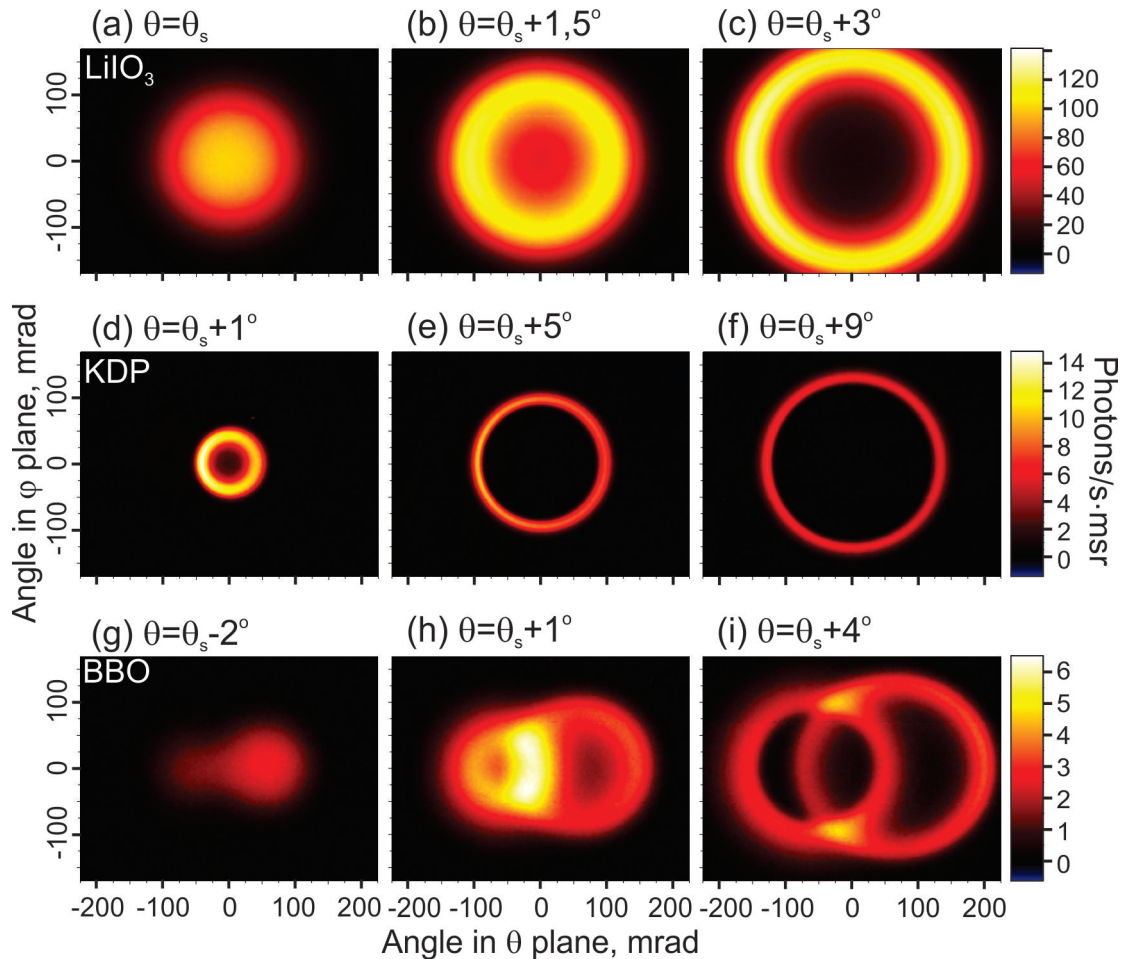


**Figure 2.3:** Angular SPDC distributions in  $\text{LiIO}_3$  (a-c), KDP (d-f) and BBO (g-i) crystals for different crystal orientation angles. In the case of  $\text{LiIO}_3$  (a-c) and KDP (d-f) crystals, the Glan prism is rotated at the angle to transmit  $e$  polarization pump radiation, in the case of BBO (g-i) crystal, the Glan prism is rotated at a  $45^\circ$  angle.

Angular distributions of SPDC excited in various nonlinear crystals are displayed in Fig. 2.3: (a - c) – pumping type I  $\text{LiIO}_3$  crystal, (d - f) – type I KDP crystal and (g - i) – type II BBO crystal. The color coding represents the detected number of photons per second emitted into  $\mu\text{sr}$  solid angle.  $\text{LiIO}_3$  and KDP crystals were excited using 0,21 mW power pump, BBO – 77  $\mu\text{W}$ . Angular distributions of SPDC in Fig. 2.3 are displayed from left to right in order of crystal angles. Nonlinear crystals orientation angle  $\theta_s$  match the scalar phase matching angle at the degeneracy:  $\text{LiIO}_3$  - 35,6°, KDP – 41,9° and BBO – 36,9°.

Comparing SPDC distributions in type I KDP (Fig. 2.3 (a - c)) and  $\text{LiIO}_3$  (Fig. 2.3 (d - f)) crystals, the differences of nonlinear media dispersion are well revealed. Phase-matching angles in KDP vary much more slowly than in  $\text{LiIO}_3$ , therefore conical radiation is less spread in the space for KDP crystal. The parametric cone widens much faster in the  $\text{LiIO}_3$  crystal than in the KDP crystal for the very same reason.

During type II nonlinear interaction in BBO crystal, two parametric cones are generated whose axes do not coincide in space and are symmetrically displaced from the pump beam in  $\theta$  plane (Fig. 2.3 (g - i)). Those angular distributions were recorded with a film polarizer rotated at 45° angle. The two cones correspond to different polarization photons ( $o$  and  $e$ ): the  $e$  polarization parametric cone is displaced to smaller crystal orientation angles while the  $o$  parametric cone is displaced with the same angle to the bigger crystal angles. In the overlapping axes of different polarization cones (Fig. 2.3 (h), (i)) conditions are created for generating entangled photons which are widely used in quantum optics experiments.

## 2.3 Power analysis of type I SPDC

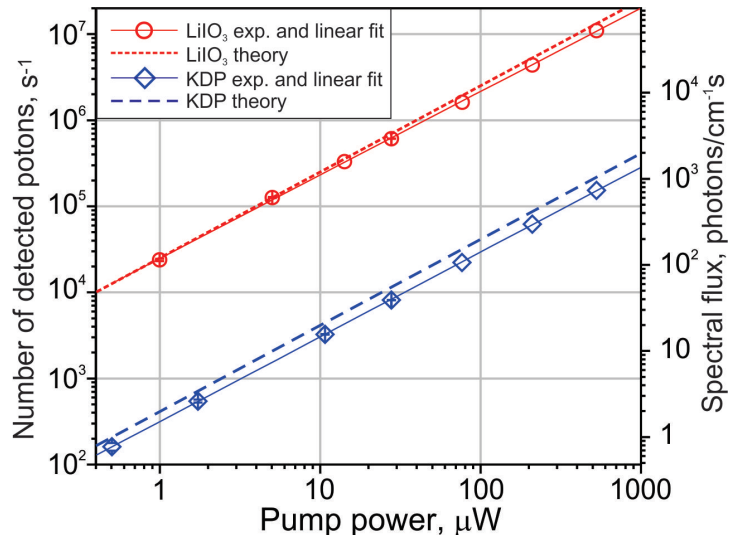


**Figure 2.4:** SPDC photon flux and spectral flux dependence on pump power in KDP (empty blue diamonds) and  $\text{LiIO}_3$  crystals (red circles); solid lines represent linear approximation of experimental values, dashed lines – simulation results.

In order to evaluate the detection system’s ability to reliably record weak SPDC signals, SPDC power dependence on the pump power was investigated (Fig. 2.4) in

type I KDP and  $\text{LiIO}_3$  crystals. The power of SPDC was obtained by integrating the spatial distribution of the SPDC. It was found that the power of SPDC pumped by incoherent sources is linearly dependent on the pump power - in our experimental conditions any other parametric processes depending on the pump intensity (such as parametric amplification) did not occur.

Fig. 2.4 shows that parametric power conversion in  $\text{LiIO}_3$  crystal is two orders of magnitude higher than in the case of KDP crystal. It is directly related to the crystal effective second-order nonlinearity: nonlinearity of  $\text{LiIO}_3$  crystal (5,2 pm/V for 800 nm wavelength) is an order of magnitude higher than KDP (0,4 pm/V for 1,064  $\mu\text{m}$  wavelength) [24]. Simulation results presented in Fig. 2.4 were obtained using an SPDC theoretical model, which was developed using formula (1.1). The model will be introduced in a subsequent section. SPDC was recorded pumping up to 0,5  $\mu\text{W}$  power pump. LED spectral irradiance is several times lower than the solar spectral irradiance.

## 2.4 Summary

In this chapter the first experimental analysis of SPDC excited by an incoherent source - high-power blue LED was presented. Angular SPDC power distributions were experimentally recorded in type I KDP and  $\text{LiIO}_3$  and type II BBO crystals. It was found that SPDC spatial properties essentially depend on the properties of nonlinear dispersive media. It was also found that the SPDC power directly depends on the pump power - it has been shown that only parametric scatter of pump photons was observed and other nonlinear processes did not occur. It should be mentioned that the capabilities of the detection system enabled us to record SPDC signal pumped up to 0.5  $\mu\text{W}$  power pump beam. In addition, the spectral irradiance of the LED was significantly lower than the spectral irradiance of the Sun. Therefore, both natural and artificial incoherent light sources can be used as an alternative to laser radiation for biphoton field excitation suitable for various applications in quantum optics. Nowadays, due to the development of optoelectronic technology, LEDs radiating in a wide optical spectrum are commercially available. This means that SPDC pumped with incoherent radiation can be used in metrology to investigate crystals effective second-order nonlinearity in a wide spectrum. Extremely cheap, compact incoherent light sources capable of emitting wide spectrum light can replace lasers in research areas where the spatial and temporal coherence of biphotons is not critical.

# 3

## Simulation of SPDC pumped by a high power LED

*Material related with this chapter was published in papers [A1, A3]*

The experimental results of SPDC pumped by blue LED revealed the ability to generate SPDC excited by incoherent light sources. SPDC power differences in KDP and LiIO<sub>3</sub> crystals can be easily explained by the difference of the crystals' effective second-order nonlinearities. On the other hand, the reasons for the spatial SPDC power distribution differences are not so trivial. Therefore, in order to qualitatively explain the differences of spatial SPDC power distributions theoretical simulations were carried out. In this chapter a theoretical SPDC model adapted for the incoherent pump beam is introduced and experimental spatial SPDC power distributions are simulated.

### 3.1 Theoretical model of SPDC excited by incoherent light sources

The theoretical model for the incoherent pump sources is based on the (1.1) formula. The key assumptions in the theoretical model development were as follows: pump depletion did not occur (parametric power conversion was approximately  $10^{-6}$ ), signal and idler waves are too weak to generate the interaction with the other waves involved in the process, pump waves do not interact with each other due to the low spatial and temporal coherency. Based on these assumptions, the pump beam can be described as a classical superposition of a plane wave and the pump power can be described as:

$$P_p(\omega_p, \varphi, \theta) = \sum_{zxy} S(\omega_{p_z}) S(\varphi_x, \theta_y) P_0; \quad (3.1)$$

here  $S(\omega_{p_z})$  and  $S(\varphi_x, \theta_y)$  are frequencies and spatial spectra distribution functions,  $P_0$  – total pump power.

SPDC signals generated by the individual pump components do not interact with each other. This opens up many possibilities for the numerical simulation to examine

the SPDC power distribution dependence on various pump and detection parameters. Total SPDC signal is the integral of the six parameters - two pump parameters which describe the propagation angles, one - the pump frequency, two parameters - the signal propagation angles and one - the signal frequency. These parameters are not independent of each other - the phase matching conditions depend on both the pump as well as the signal frequency and propagation direction, so during the initial integration the order of parameters is important. However, the SPDC power distribution function for all six parameters which is the result of the initial integration can be analyzed for the freely selected initial conditions. The order of the parameters during the integration of the SPDC power distribution function become unimportant. The desired pump and signal spectral components can be freely chosen independently of the amount of the other interacting components. Using the SPDC pumped by the plane monochromatic wave power expression (formula (1.1)) SPDC pumped by the incoherent radiation power expression can be written:

$$P_s = P_0 L^2 \sum_{zxy} S(\omega_{p_z}) S(\varphi_x, \theta_y) \int_0^\infty \int_{-\pi/2}^{\pi/2} \int_{-\pi/2}^{\pi/2} \frac{\omega_s^4 \omega_i d_{ef}^2 \hbar n_s}{4\pi^3 \epsilon_0 c^5 n_i n_p} \text{sinc}^2 \frac{\Delta k L}{2} q(\omega_s) d\varphi d\theta d\omega_s. \quad (3.2)$$

here  $q(\omega_s)$  – detection quantum efficiency function, equal to a product of all optical elements used in detection system transmission functions and photon counter quantum efficiency function.

A unique software code was developed with MATLAB scientific computing software using formula (3.2). Simulations were performed in KDP, LiIO<sub>3</sub> and BBO crystals whose dispersion properties are described using Sellmeier formulas from D. N. Nikogosyan book [24]. Temporal and spatial pump beam distribution in the theoretical model was equivalent to the experimental conditions. The simulation results are SPDC angular distribution in  $\theta$  plane. The quality of simulation depends on the discretization step size and computation time. The main result of the simulation is a data "cube" in which the biphoton flux - parametric cone waves power distribution over pump and signal spatial and temporal frequencies is recorded. SPDC power distribution is represented using this data cube: the parametric power distribution over the pump and detection both spatial and temporal spectra is displayed, and total parametric power is calculated.

### 3.2 Theoretical characterization of the experimental SPDC power distribution

In order to apply SPDC excited by incoherent radiation in quantum optics or other research areas, it is important to be able to define and modify the spatial distribution of the SPDC waves. Therefore, a theoretical and experimental analysis of the spatial SPDC power distribution dependence on the temporal and the spatial pump beam spectra was performed (Fig. 3.1). A 24 nm (FWHM) spectral width and 38 mrad (FWHM) width of the spatial spectrum pump beam was used. The



theoretical simulation was performed narrowing only one type of spectrum – either spatial or temporal.

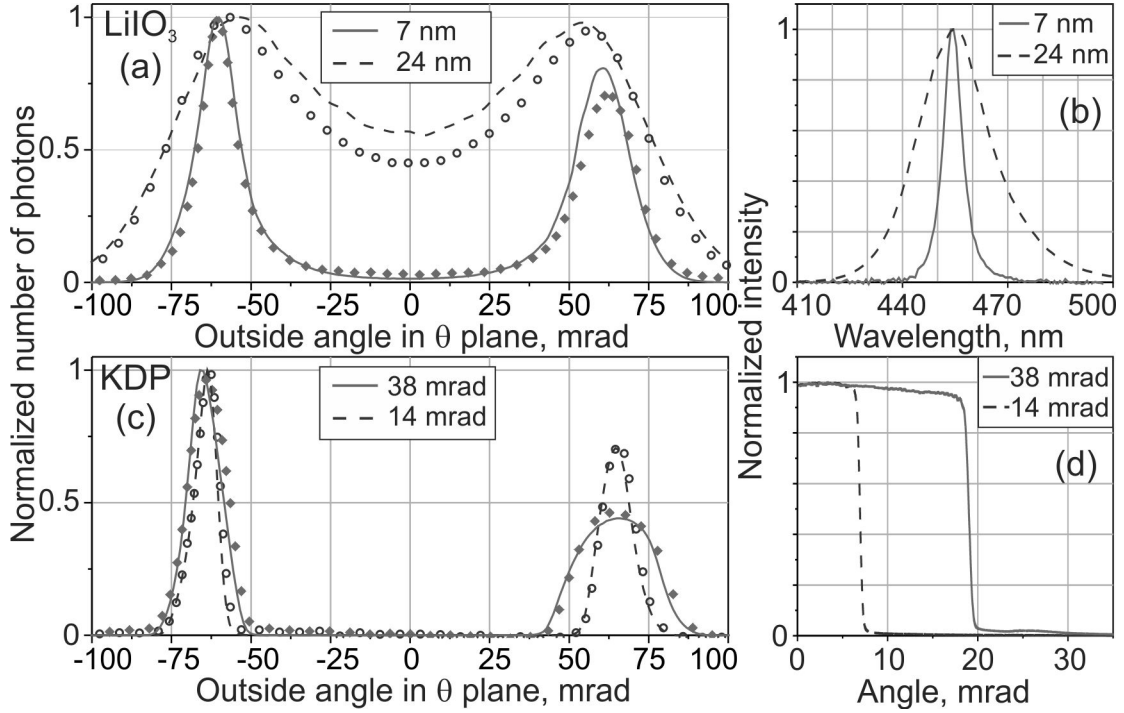


**Figure 3.1:** Cross-sections of SPDC spatial power distributions: (a) exciting  $\text{LiIO}_3$  crystal with different spectral width radiation and (c) exciting KDP crystal with different spatial spectrum width radiation. (b) pump beam frequencies spectra used for the  $\text{LiIO}_3$  crystal excitation, (d) pump beam spatial spectra used for the KDP crystal excitation.

Performing the simulation, it was found that in the case of  $\text{LiIO}_3$  crystal SPDC power distribution practically does not depend on the spatial spectrum of the pump, but varies substantially as the width of the pump frequency spectrum narrows from 24 nm to 7 nm (Fig. 3.1 (a - b)). Narrowing the pump temporal spectrum SPDC power distribution in  $\text{LiIO}_3$  crystal more and more localizes into a narrow conical radiation and the asymmetry of the SPDC power distribution increases: right-hand SPDC cone wall spectral intensity becomes lower than the left-hand. Spatial distribution of the SPDC power in KDP crystal does not vary as the temporal spectrum of the pump narrows, but is modified by diminishing the pump beam spatial spectral width from 38 mrad to 14 mrad (FWHM) (Fig. 3.1 (c - d)). Asymmetry of the SPDC cone decreases for the narrower pump spatial spectrum.

SPDC power components were analyzed in a three-dimensional data cube in which the axes correspond to the radial pump spatial spectrum, pump temporal spectrum and detection spatial spectrum in  $\theta$  plane. Choosing different data cube cut directions it is possible to analyze how SPDC biphoton field properties depend on the various parameters. The main simulation results are shown in Fig. 3.2. They consist of three pictures for each crystal: spatial spectrum of the biphoton field in phase matching  $\theta$  plane dependence on the pump temporal (a-c) and radial spatial spectrum (d-f) and the integral spatial spectrum of the biphoton field in phase matching  $\theta$  plane (g-i). Nonlinear crystals were chosen equivalent to the experimental conditions (Fig.

2.3 (b), (e) ir (i)): 20 mm type I KDP crystal, oriented by  $\theta=46,9^\circ$  angle (spatial SPDEC power distribution corresponds the Fig. 2.3 (e)), 20 mm type I  $\text{LiIO}_3$  crystal, oriented at  $\theta=37,1^\circ$  angle (Fig. 2.3 (b)) and 8 mm type II BBO crystal, oriented at  $\theta=40,9^\circ$  angle (Fig. 2.3 (i)).

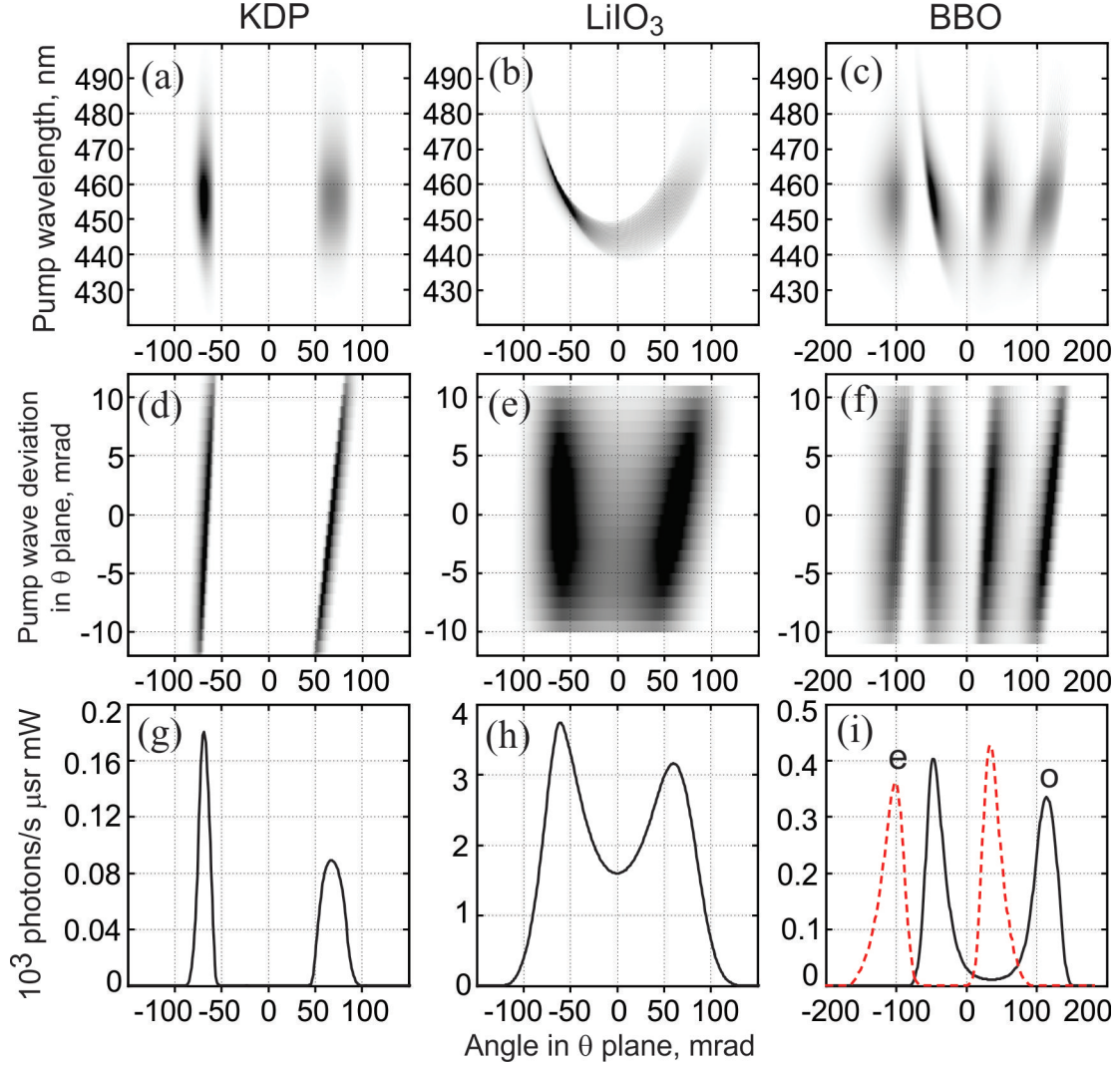


**Figure 3.2:** Theoretical SPDC pumped by the blue LED power distributions for KDP (a, d, g),  $\text{LiIO}_3$  (b, e, f) and BBO (c, f, i) crystals. In (a - c) angular SPDC power distribution dependence on the pump wavelengths is displayed, (d - f) – angular SPDC power distribution dependence on the pump waves angle in the phase-matching plane, (g - i) – SPDC power distribution cross-section in the phase-matching plane; here *e* (red dashed line) – extraordinary polarization, *o* (black solid line) – ordinary polarization SPDC beam. Angles correspond to the internal angles in nonlinear crystals.

In the KDP case, asymmetry of the biphoton field spatial spectrum (Fig. 3.2 (g)) emerges due to the strong phase matching angles dependence on the pump spatial spectrum (Fig. 3.2 (d)). In the  $\text{LiIO}_3$  case, the pump temporal spectrum has the major impact on the SPDC spatial distributions (Fig. 3.2 (b)). With an increase in the pump wavelength, the biphoton field radiation changes from a broad axial (for  $\sim 445$  nm pump wave, Fig. 3.2 (b)) to a broad conical (for  $\sim 460$  nm pump wave) radiation. In type II BBO crystal, while the pump wavelength increases (Fig. 3.2 (c))

the  $e$  polarization parametric cone width does not change while the  $o$  polarization parametric cone width increases [25]. As the pump spatial spectrum width increases (Fig. 3.2 (f)) both  $o$  and  $e$  polarization cones width increases [26]. In other words, narrowing only the spatial spectrum or only the temporal spectrum does not have a major impact on the spatial coherence of SPDC radiation in type II BBO crystal.

### 3.3 Summary

In this chapter the theoretical model used for the analysis of SPDC power spatial distribution pumped by incoherent radiation was introduced. It was found that the SPDC power spatial distribution is determined by the individual dispersion characteristics of the nonlinear media. Spatial properties of SPDC radiation generated in the KDP crystal are mainly determined by the pump beam spatial spectrum, while in the  $\text{LiIO}_3$  case the dominant influence is made by the pump temporal spectrum. High spatial biphoton field coherency in the KDP crystal may give optimistic expectations for the incoherent radiation wide applications as a pump source for biphoton field generation. However, in the BBO crystal, which is one of the most popular nonlinear crystals for biphoton field generation in quantum optics, the creation of a spatially coherent biphoton field is not possible by narrowing only the spatial or only the frequency pump spectrum. In order to generate a qualitative biphoton field in type II BBO crystals, it is best to use laser radiation as the pump source, with which it is possible to achieve high spectral irradiance and high temporal coherence of the biphoton field. On the other hand, results of the theoretical simulation showed that, in some cases, incoherent radiation can be applied to spatially qualitative SPDC generation.

# 4

## Statistical analysis of a biphoton field excited by a blue LED

*Material related with this chapter was published in paper [A4]*

Since the first statistical experiments, photon number distribution measurements are usually carried out in order to fully describe the statistical properties of the light field [27]. In the scientific literature, the light field photon distributions are usually compared with the Poisson statistics describing the coherent light field. Poisson distribution variance is equal to the mean value ( $\sigma^2 = \mu$ ) [28]. When the variance is greater than the average ( $\sigma^2 > \mu$ ), we have a super-Poisson distribution - the classical thermal light, when lower ( $\sigma^2 < \mu$ ) - sub-Poisson distribution - non-classical light [29–31]. There are many ways to generate non-classical light: the fluorescence of a single atom or ion, quantum dots in semiconductors [29], as well as the SPDC. For this reason, biphoton field statistics studied in various scientific laboratories are commonly described by sub-Poisson distribution [32–35]. While using a classical light field for biphoton field excitation, the question appears as to whether the statistics of this biphoton field differ from the biphoton field excited by laser radiation. In this chapter, the statistical properties of a biphoton field excited by incoherent radiation and the detectors afterpulses influence on the light field statistical properties will be analyzed.

### 4.1 Experimental setup

The experimental setup for the biphoton field statistical analysis is displayed in Fig. 4.1. Modified blue LED radiation was used for the biphoton field excitations, with central wavelength 404 nm and spectral width FWHM=14 nm. A pump beam was formed using lenses and irises system forming 0,8 mm diameter and three different spatial spectrum (9, 15 and 40 mrad) beam. The biphoton field is generated in a 2 cm length  $\text{LiIO}_3$  crystal, oriented at  $43,4^\circ$  with respect to the pump beam. Two

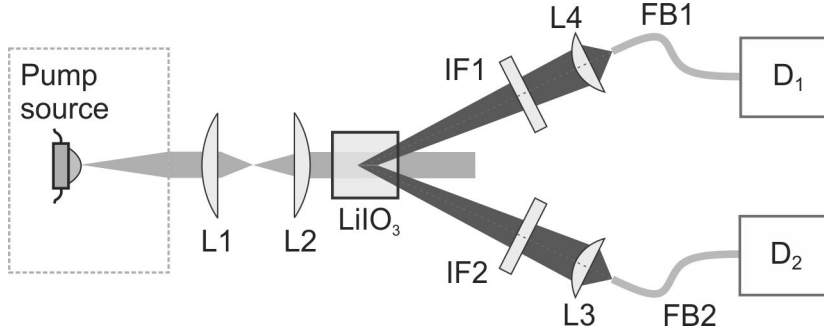


**Figure 4.1:** Experimental setup for the biphoton field statistical analysis, here L1 - L4 - lenses, IF1 and IF2 – interference filters in the first and second detection channels, FB1 ad FB2 - fibers. D<sub>1</sub> and D<sub>2</sub> - photon counters.

detection channels were chosen in the biphoton field cone. Detection channels are placed on the opposite cone walls symmetrically at a 50 mrad angle from the pump beam axis in noncritical phase matching  $\phi$  plane. The signal is coupled to D<sub>1</sub> and D<sub>2</sub> photon counters using multimode fibers. 38,5 nm spectral width interference filters (IF1 and IF2) are used in the detection channels. The photon counters detection time interval was chosen at 20  $\mu$ s.

## 4.2 Research on the biphoton statistical distribution

Photon number measurement in both detection channels showed that with the increase of the pump spatial spectral width, the average recorded photon number increases (9 mrad case - 0,023 photons/element, 15 mrad - 0,061 photons/element, 40 mrad - 0,447 photons/element). It was expected that the photon statistics in both detection channels would be multimode, reflecting the detector Poisson distribution. Analysis of the data with the Matlab software Pearson chi-square test package showed that the distribution of the biphotons does not satisfy the Poisson distribution. We observed experimentally only the SPDC process, therefore it was predicted that the deviation from the Poisson distribution is determined by the statistical properties of the detector. In order to determine the detector influence on statistical distribution, it was decided to investigate the photon sample statistics using a negative binomial distribution function, which also can describe the multimode radiation. The negative binomial distribution describes the distribution of the events which we do not expect:

$$f(k) = \frac{\Gamma(k+r)}{\Gamma(k+1)\Gamma(r)}(1-p)p^k \quad (4.1)$$

here  $\Gamma(x)$  - Gamma function,  $r$  – number of failures until the experiment is stopped and  $p$  - success probability in each experiment. Negative binomial distribution parameters  $r$  and  $p$  do not describe directly properties of the light field, therefore the distribution mode parameter was introduced:

$$N_{modes} = \frac{1}{1-p} \quad (4.2)$$

The statistical parameters of the biphoton field excited by the different spectral width pump beam and recorded with both detectors are shown in Table 4.1. It can be clearly seen that the values of the distribution mode parameter differ greater for the different detectors.

**Table 4.1:** Biphoton field statistical parameters:  $r$  - number of failures until the experiment is stopped,  $p$  - success probability in each experiment,  $N_{modes}$  - photon number distribution mode parameter.

Detection channel number	Pump spatial spectrum width	$r$	$p$	$N_{modes}$
$D_1$	9 mrad	4,54	0,9949	196
	15 mrad	11,2	0,9945	181
	40 mrad	111	0,996	250
$D_2$	9 mrad	0,77	0,968	31,6
	15 mrad	2,41	0,972	35,8
	40 mrad	18,5	0,973	37

The very large mode parameter difference is determined by the detector afterpulse generation probability, which often distorts the recorded light statistical properties [36, 37]. In order to find the afterpulse probability and the negative binomial distribution mode parameter correlation a theoretical simulation was performed. First of all, we numerically simulated the Poisson distribution photo events sequence, that sample size and the average number of photo events are equivalent to the experimental photon distribution. The simulated photo event sample was modified by randomly adding secondary photo events with an afterpulse generation probability. The negative binomial distribution was adapted for the modified photo events sample and the distribution mode parameter was determined. The simulation showed that the mode parameter is inversely proportional to the probability of afterpulse generation. Based on the simulation results it was determined that the mode parameter in the first detection channel  $D_1$  is equivalent to 0.31% afterpulse generation probability and in the second channel  $D_2$  - 1,9%. These values match those supplied by the detector manufacturers.

### 4.3 Summary

Summing up the statistical analysis of the experimental biphoton field excited by the blue LED, we can say that the temporal resolution of the experimental conditions was not sufficient to qualitatively record biphoton statistical properties. The distribution mode parameter was introduced, which allows us to quantitatively determine the avalanche photodiodes afterpulse generation probability. Numerical simulation showed that the mode parameter decreases with increasing afterpulse probability. This law is not universal, but depends on the average number of photo events in the detection channel. It was also found that by using the photon counters a sufficiently large photon flux could be registered that photon coincidence studies could be performed on the biphoton field excited by incoherent radiation.

# 5

## Research on SPDC excited by a blue LED in $\text{LiIO}_3$ crystal photon coincidences

*Material related with this chapter was published in papers [A2, A4]*

For many decades SPDC has been applied in quantum optics as an entangled photon source, exciting a nonlinear medium by coherent laser radiation. Nonlinear interactions at both temporal and spatial properties of the laser radiation coherence are transmitted directly to the biphoton radiation via nonlinear interaction. Research on experimental and theoretical SPDC excited by incoherent radiation revealed that, under certain conditions, high spatial biphoton coherence can be achieved. This raises a natural question: is it possible to apply this type of radiation in quantum optics experiments? This section presents the methodology for recording the photon coincidences and presents experimental results of photon coincidences when exciting the  $\text{LiIO}_3$  crystal with a blue LED.

### 5.1 Principles of photon coincidence measurements

One of the main biphoton field characterization methods is photon coincidence counting. Photon detection is performed with two photon counters from the specific directions where the twin photon flux propagates in as narrow as possible time window, and the photon coincidences - the number of photons recorded by both detectors in the same time window - are counted [14]. Optimal directions in which photon coincidence measurements can be carried out are schematically displayed in Fig. 5.1. In type I SPDC case (Fig. 5.1 (a)) the opposite direction on the cone walls in  $\varphi$  plane are selected, as in this case twin photons are scattered symmetrically on opposite sides of the pump photon flux. In type II SPDC case photon coincidences are recorded in the directions in which the two light cones intersect (Fig. 5.1 (b)), because in those directions entangled photon states are created.

Usually the photon coincidence measurement time window is set to several nanosec-

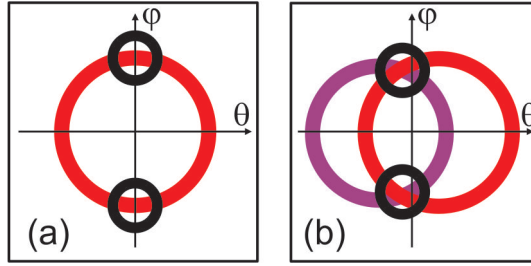


**Figure 5.1:** SPDC photon coincidence measurement scheme for type I (a) and type II parametric interaction (b); here black circles – detection areas. Photon counts detection areas for the type II interaction (b) were chosen in the directions, where the entangled photons propagate.

onds [38, 39]. It should be longer than the twin photons’ coherence time, which is usually as long as tens of femtoseconds [40]. On the other hand, the coincidence time window should be as short as possible to avoid accidental coincidences that can be analytically estimated as [41]:

$$A_{1,2} = N_1 N_2 (\tau_1 + \tau_2); \quad (5.1)$$

here  $N_1$  and  $N_2$  – photon number in the first and the second detection channel,  $\tau_1$  and  $\tau_2$  – detection time intervals in the first and the second detection channel.

## 5.2 Experimental setup

The experimental setup for the SPDC pumped by blue LED photon coincidence measurement is displayed in Fig. 5.2. A high spectral irradiance blue LED was used as a pump source. Total LED power was 0.9 W, central wavelength – 403.5 nm, spectral width (FWHM) 14.4 nm. Both pump spatial spectrum and pump beam diameter in an experiment were changed discreetly: 9, 15, 25 or 40 mrad pump spatial spectrum and 0.8, 1.8, 3, 5 or 8 mm diameter beam were formed. Pump power varied from 1.64  $\mu$ W to 3.26 mW; spatial pump power distribution was practically uniform. A 2 cm type I LiIO<sub>3</sub> crystal was used for the biphoton field generation, oriented at a 43.4° angle with respect to the pump beam. A Glan polarizer in the pump source was used to linearly polarize the pump beam. It was also used for registering the background - choosing pump waves *o* polarization, which do not take part in the nonlinear SPDC interaction.

Two directions for photon detection were chosen in the opposite 0,1 rad angle light cone walls (Fig. 5.1 (a)), symmetrically propagating 50 mrad from the pump beam axis in non-critical phase matching  $\varphi$  plane. Two identical detection channels were formed in those directions, consisting of 37.5 nm spectral width interference filters IF1 and IF2, transmitting the radiation in degeneracy range, and L5 and L6 lenses, with which parametric radiation was coupled into fibers. In the experiment, we used a step refraction index 105  $\mu$ m core diameter, NA=0.22 numerical apertures multimode fibers, with which the signal was coupled into PerkinElmer Inc. D<sub>1</sub> and D<sub>2</sub> photon counters (SPCM-AQRH-14-FC). TTL pulses emitted from the photon counters were directed into a coincidence circuit with a coincidence window of 7 ns.



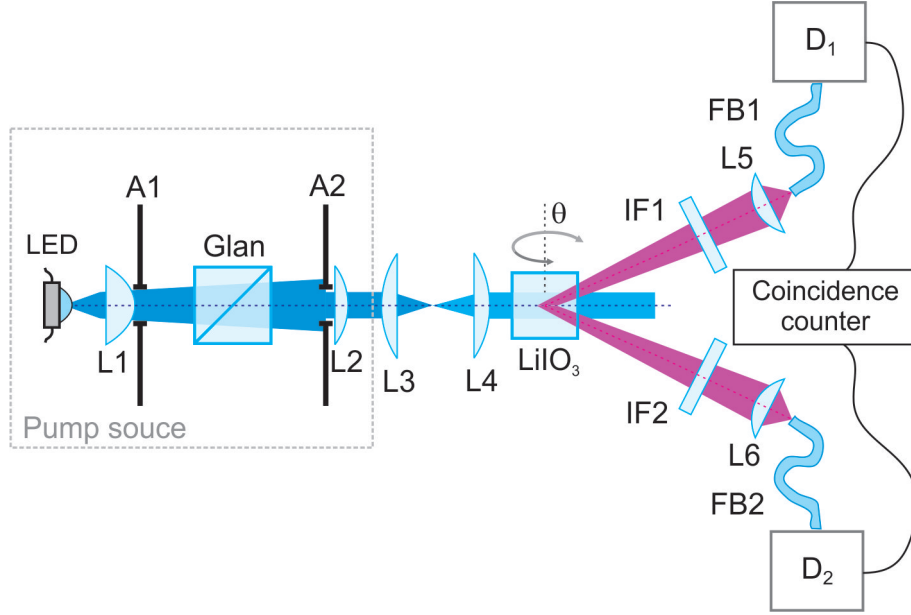


**Figure 5.2:** Experimental setup of the SPDC pumped by blue LED photon coincidence measurement; A1 and A2 - irises, L1 - L6 - lenses, Glan - Glan polarizer, IF1 and IF2 – interference filters in the first and the second detection channel, FB1 and FB2 - fibers,  $D_1$  and  $D_2$  - photon counters.

### 5.3 Coincidence results for twin photons pumped by different parameter pump beams

Fig. 5.3 presents the main measurement results: single photon flux (a) and photon coincidences flux (b) dependence on the pump power and the pump beam parameters. The single photon flux value is the average value of single-photon fluxes recorded in both photon counters with subtraction of the detectors dark counts and background fluorescence. The photon coincidences flow corresponds to the photon number overlapping coincidence time window in both detection channels. It is recorded with the subtraction of the accidental coincidences calculated using (5.1) formula. The experimental values are connected with curves corresponding to the same pump parameter; the black curve connects points corresponding to the constant pump diameter, the violet curve – constant spatial pump spectrum.

It was determined that the single photon flux is directly proportional to the pump power, which depends on the square of the spectral pump width (Fig. 5.3 (a)). Photon coincidences also depend on the square of the spectral pump width for a small and medium divergence of the pump beam but for the higher spectral pump width values photon coincidences start to increase more slowly than the single photon flux (Fig. 5.3 (b)). Comparing the influence of the pump beam diameter, it was found that, with the increasing pump beam diameter, the single-photon flux increases approach saturation. Photon coincidences also increase with the pumping beam diameter, but reach saturation more quickly than the single photon flux.

The quality of the photon coincidences is determined by the photon coincidence ratio, which describes what part of a single photon flux takes the photon coincidences:  $C = \frac{N_{coin}}{N_{singles}}$ , here  $N_{coin}$  - number of photon coincidences,  $N_{singles}$  - number of single photons. Using the smallest divergence and the smallest diameter pump

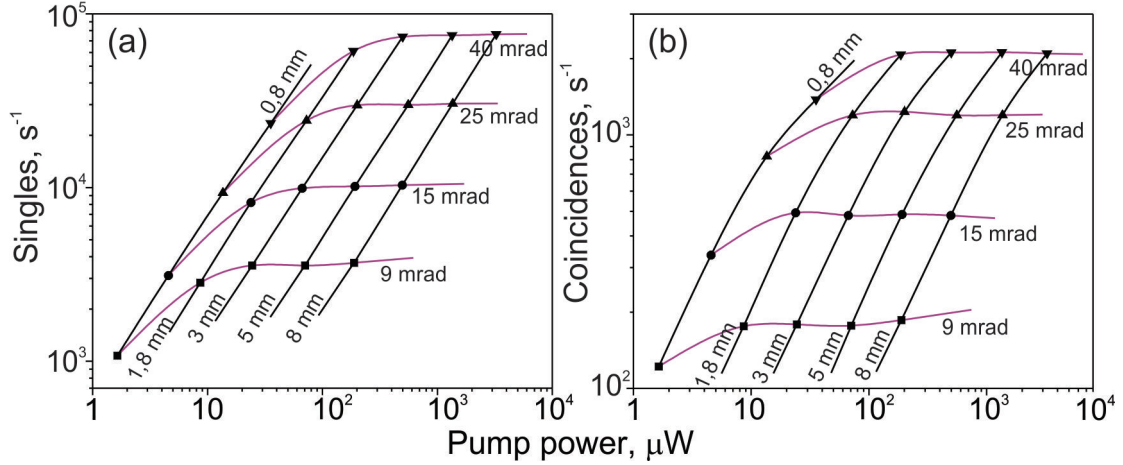


**Figure 5.3:** Singles (a) and photon coincidences (b) flux dependence on the pump power for the different characteristics of the pump beam. Black curves join the constant pump beam diameter (0,8, 1,8, 3, 5 and 8 mm) values, violet curves join the constant pump beam spatial spectrum (9, 15, 25 and 40 mrad) values.

beam an 11.5% photon coincidence ratio was achieved, because the narrow and low divergence pump beam nonlinear interaction volume is coupled the most effectively into detection channels. This corresponds to 49% of photon coincidence ratio if the detection system were ideal – no optical losses would exist in any optical elements and detector quantum efficiency would be maximum (100%). Using a large diameter (5 and 8 mm) pump beam, the photon coincidence ratio evenly decreased (from 5% to 2.8%) while increasing spatial spectrum of the pump. The reason is that spatial scattering of the twin photons increases and a smaller number of photon coincidences are coupled into the detection channels.

While changing the spatial position of the detector, it was found that photon coincidence ratio dependence on the detectors position is bell-shaped for the biphoton field excited by the 25 mrad divergence and 5 mm diameter pump beam. Photon coincidence ratio varies considerably faster when changing the position of the detector in  $\theta$  plane (FWHM = 125  $\mu\text{m}$ ), in which the photon coincidence area is directly limited by multimode fiber core, than in  $\varphi$  plane (FWHM = 245  $\mu\text{m}$ ). When changing the crystal angle with respect to the pump beam, it was found that both single photon flux and photon coincidences are not sensitive to the crystal orientation compared with the biphoton field pumped by laser radiation. Half width (FWHM) of single photon flux dependence on crystal angle function is  $2.1^\circ$ , photon coincidences –  $1.3^\circ$ .

In order to determine photon coincidence flux in one spatial mode, measurements were performed using a single-mode and multimode fiber. An average spatial properties (25 mrad divergence and 5 mm diameter) pump beam was used. The multimode fiber FB1 (Fig. 5.2) used in the first detection channel was replaced by the single-mode fiber Thorlabs 780 HP, with 5  $\mu\text{m}$  core diameter and NA=0.13 numerical aperture. Single photon flux was 17.5 photons/s (in the multimode fiber case –  $29 \cdot 10^3$  photons/s – 1650 times bigger). Comparing the fiber diameter and the numerical aperture, it can be evaluated that the single-mode fiber acceptance area is 1270 times smaller than the multimode fiber. The single photon flux drop is

very close to this value, therefore it can be concluded that the biphoton field is distributed evenly in the detection space. Photon coincidences for the one single-mode and one multimode fiber case were 1.31 coincidences/s (in two multimode fibers case - 1230 coincidences/s. The photon coincidence ratio for the one single-mode and one multimode fiber significantly increased (from 4.2% to 7.5%).

## 5.4 Summary

In this chapter, the first photon coincidences results for an experimental biphoton field excited in  $\text{LiIO}_3$  crystal by incoherent radiation were analyzed. It was found that the single photon flux linearly proportional to the pump power broadening the pump spatial spectrum. Single photon flux depends on the pump beam diameter in the following way: it significantly grows only for small diameter values (0.8 and 1.8 mm) and saturates for the bigger diameters of pump beam. The photon coincidence flux essentially duplicates the characteristics of the single photon flux variations. The single photon flux (1077 photons/s), the photon coincidences (122 coincidences/s) and the photon coincidence ratio (11,5%) recorded with the smallest pump power are large enough that the incoherent pump radiation would be a perspective pump source for medium quality biphoton field excitation and its application in various quantum optics experiments.

Photon coincidence ratio dependence on the detector position is bell-shaped; the effective photon coincidence detection area in  $\varphi$  plane is twice wider than in  $\theta$  plane. Orientation of the nonlinear medium with respect to the pump beam is not critically important. Photon coincidence measurements using multimode and single-mode fibers showed that the single photons (17.5 photons/s) and the photon coincidence flux (1.31 coincidences/s) are big enough to be successfully registered.

# 6

## Theoretical analysis of a biphoton field excited by incoherent radiation

*Material related with this chapter was published in papers [A2-A4]*

Experimental results for photon coincidences excited by incoherent radiation provide high hopes for applying the incoherent sources in entangled photon experiments. In order to find the optimal pump and detection systems characteristics for achieving the highest quality biphoton field, a nonlinear response of incoherent radiation in various nonlinear media was theoretically analyzed. In this section, a theoretical model for the twin photon coincidences will be presented. The spatial SPDC distributions in LiNbO<sub>3</sub>, LiIO<sub>3</sub> and BBO crystals excited by broadband incoherent radiation will be examined. Experimental biphoton field photon coincidences in LiIO<sub>3</sub> crystal results presented in the previous chapter will be theoretically analyzed.

### 6.1 Theoretical model of the SPDC photon coincidences

Photon coincidences are theoretically analyzed using the modified theoretical model for SPDC power distribution introduced in chapter 3.1. In this model, the interaction between pump components is not taken into account and it is assumed that the pump beam is a linear superposition of pump waves involved in nonlinear interaction ((3.1) formula). The biphoton SPDC field is a linear superposition of separate SPDC waves generated by each pump component ((3.2) formula). In the theoretical model, spatial filtering for photon detection is applied - a circular detection area mask is created - a matrix of 0 and 1, where 1 denotes the spatial region in which the photon flux is registered, 0 - the area in which the photon flux is not registered. During integration of the total photon flux, a mask is positioned in the selected point in space and is applied to each signal component separately. The photon coincidence flux is directly dependent on the detection space position and size of

the detection area, therefore the detection channel parameters can be selected only before the initial integration. After the initial integration, single photon and photon coincidence flux density matrixes for 6 parameters are created. Further analysis can be carried out in freely selected initial conditions. The desired pump and signal spectral components can be freely chosen.

Using (3.2) formula the equation for the single photon number in the detection channel calculation can be written down:

$$N_{s,i} = \int_0^\infty \frac{L^2}{\hbar\omega_{s,i}} \int_{\pm\theta_D-\psi_{det}}^{\pm\theta_D+\psi_{det}} \int_{\varphi_D-\psi_{det}}^{\varphi_D+\psi_{det}} P(\omega_p, \varphi, \theta) \beta S(\varphi_D, \pm\theta_D, \psi_{det}) q(\omega_{s,i}) \text{sinc}^2\left(\frac{\Delta k L}{2}\right) d\varphi d\theta d\omega_{s,i}; \quad (6.1)$$

here  $L$  – length of the nonlinear medium,  $\omega_{s,i}$  – signal or idler wave frequency,  $P(\omega_p, \varphi, \theta)$  – pump beam distribution described by the (3.1) formula,  $\beta$  – parametric conversion coefficient,  $S(\varphi_D, \pm\theta_D, \psi_{det})$  – detection space mask function, where  $\psi_{det}$  – spatial spectrum radius,  $(\varphi_D, \pm\theta_D)$  – detectors position in spatial coordinates,  $q(\omega_{s,i})$  – detectors quantum efficiency,  $\Delta k$  – phase mismatching,

Calculating the phase-matching conditions in the theoretical simulation, we can describe the idler photons spatial position and calculate what number of idler photons, twinned with signal photons, are recorded in the detection channel. This allows us to spatially relate the twin photons and theoretically investigate the photon coincidences – to calculate the number of idler photons recorded in the second detection channel which are related with the signal photons recorded in the first detection in  $[\omega_{s1}, \omega_{s2}]$  frequency range. The first detection channel is described by the coordinates  $(-\theta_D, \varphi_D)$  and angular width  $\psi_{det}$ , the second channel –  $(\theta_D, \varphi_D)$  and  $\psi_{det}$ . Photon coincidence ratio  $C$  is calculated by dividing the photon coincidences number by the number of single photons detected in the second detection channel in  $[\omega_{s1}, \omega_{s2}]$  spectrum range. This condition in the theoretical model is described with Heaviside step function  $H(\omega_i - \omega_{s1})$  and  $H(\omega_{s2} - \omega_i)$ , here  $\omega_i$  – idler wave frequency. The total photon coincidence ratio can be expressed:

$$C(\omega_p, \varphi, \theta) = \frac{\int_{\omega_p-\omega_{s2}}^{\omega_p-\omega_{s1}} \frac{L^2}{\hbar\omega_i} H(\omega_i-\omega_{s1}) H(\omega_{s2}-\omega_i) \int_{-\theta_D-\psi_{det}}^{-\theta_D+\psi_{det}} \int_{\varphi_D-\psi_{det}}^{\varphi_D+\psi_{det}} \beta S(\varphi_D, -\theta_D, \psi_{det}) q(\omega_i) \text{sinc}^2\left(\frac{\Delta k L}{2}\right) d\varphi d\theta d\omega_i}{\int_{\omega_{s1}}^{\omega_{s2}} \frac{L^2}{\hbar\omega_s} \int_{\theta_D-\psi_{det}}^{\theta_D+\psi_{det}} \int_{\varphi_D-\psi_{det}}^{\varphi_D+\psi_{det}} \beta S(\varphi_D, \theta_D, \psi_{det}) q(\omega_s) \text{sinc}^2\left(\frac{\Delta k L}{2}\right) d\varphi d\theta d\omega_s}. \quad (6.2)$$

The numerator of the photon coincidence ratio can be understood as the number of signal and idler photon twins whose distribution functions overlap in spectral and spatial area ( $N_i \cap N_s$ ):

$$C = \frac{N_i \cap N_s}{N_s}. \quad (6.3)$$

Those equations ((6.2), (6.3)) express the quality of the biphoton field – the probability of recording the photon coincidences in a particular coincidence time window using ideal photon detectors.

### 6.1.1 Geometric factor

Equations for the single photon ((6.1) formula) and photon coincidence ((6.2) formula) fluxes were written down considering that all pump components participate in the nonlinear interaction. However in reality, the wide pump beam occupies a particular volume of the nonlinear medium and just a part of the interaction volume is coupled into the detectors. In order to qualitatively and quantitatively evaluate the experimental photon coincidence results, pumped by incoherent radiation, the concept of the geometric factor was introduced describing the ratio of space coupled into the detector and nonlinear interaction space. Those spaces are visually displayed in Fig. 6.1.

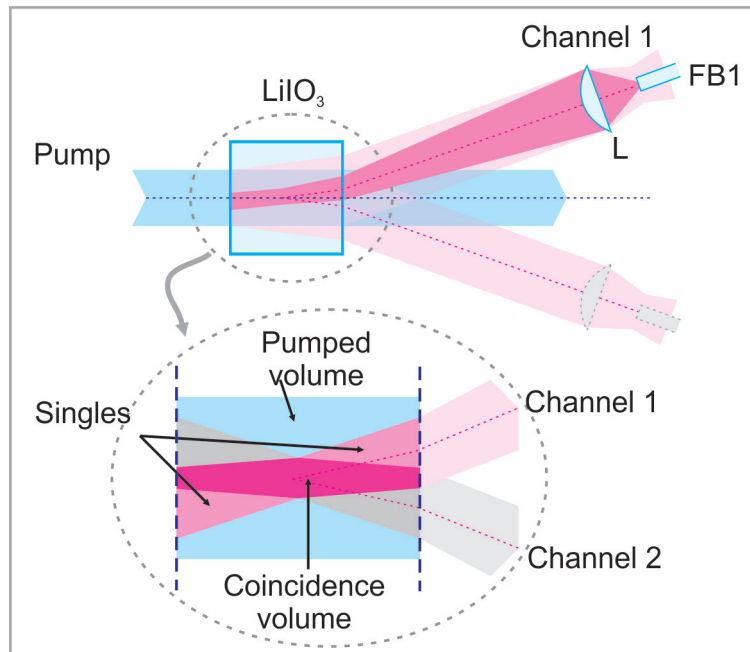


**Figure 6.1:** Model of the geometric factor for the single photons and photon coincidences calculations; here L - lens, FB1 – fiber in the first detection channel.

In the geometric factor calculation, we consider that the pump beam is uniform and has a rectangular shaped spatial distribution, space in all the crystal volume is uniformly coupled into the detection channel, the detection space is limited by the numerical aperture of imaging lenses and optical fibers. The ideally nonlinear medium coupled spaces into detectors are shown in Fig. 6.1 as red areas. The 1.05 mm diameter nonlinear medium space is coupled into multimode optical fiber in our experimental conditions. We used quite wide pump beams (from 0.8 to 8 mm diameter), therefore the usually nonlinear interaction space, limited by the pump beam (shown as blue in Fig. (6.1), was much larger than the space coupled into the detectors. The geometric factor of single photons is equal to the ratio of interaction volume ( $V_j \cap V_k$ ) coupled into detection channel  $j$  to nonlinear interaction volume ( $V_k$ ). The number of single photons is expressed:

$$N_j = \frac{V_j \cap V_k}{V_k} N_s. \quad (6.4)$$

The geometric factor of photon coincidences is equal to the overlap ratio of vol-

umes coupled into both detection channels to the nonlinear interaction volume. The number of photon coincidences is expressed:

$$C_{12} = \frac{V_1 \cap V_2 \cap V_k}{V_k} C. \quad (6.5)$$

## 6.2 Theoretical simulation of a broadband biphoton field excited in dispersive media

To determine the differences between biphoton fields, the incoherent and coherent radiation characteristics of a biphoton field excited in a LiNbO<sub>3</sub> crystal were analyzed. Three cases were studied (Fig. 6.2): with uniform power distribution both in frequencies and spatial spectra incoherent radiation exciting a 1 mm (Fig. 6.2 (a)) and 10  $\mu$ m (Fig. 6.2 (c)) length LiNbO<sub>3</sub> crystal, and with uniform power distribution over spatial spectrum monochromatic radiation exciting a 1 mm length LiNbO<sub>3</sub> crystal (Fig. 6.2 (b)). Biphoton distributions are displayed in Fig. 6.2 both in detection (a-c) and in pump (d-f) spatial and frequencies spectra. Biphoton density in this case is described as parametric wavenumbers ( $k_s$  and  $k_i$ ) density. In Fig. 6.2 (a-c) vertical axis biphoton propagation angles are plotted with respect to LiNbO<sub>3</sub> crystal which is oriented in 90° synchronism.

The twin photon density distribution shows which pump spectral part is responsible for the biphoton generation (Fig. 6.2 (d - f)). It is noticeable that biphotons from the narrow frequencies spectral band can be spread over a large spatial area. This biphoton characteristic is best expressed in the coherent pump case (Fig. 6.2 (a) and (c)). On the other hand, biphotons pumped by coherent radiation (Fig. 6.2 (b)) can be distributed in the wide frequencies band but are well localized in the narrow propagation angles range. The spatial distribution of photon pairs is important when the biphoton field transformation is analyzed in the example of second harmonic generation [19]. Biphotons pumped by coherent radiation maintain a coherent relation with each other and, in the second harmonic generation case, the pump beam could be reconstructed. The second harmonic generation from the biphotons pumped by incoherent radiation would generate photons in a much wider spatial area, therefore it would provide much more capability for reforming spectral characteristics of the pump radiation.

We should now discuss the photon coincidence dependence on the detection channels' spatial and frequencies spectral width. As the pump source the blue LED will be chosen emitting 456 nm central wavelength, 24 nm (FWHM) spectral width, 19 mrad spatial spectral width radiation. A biphoton field is excited in type I  $\theta = 37.1^\circ$  LiIO<sub>3</sub> and type II  $\theta = 40.9^\circ$  BBO crystals. The detection area in the theoretical model is determined by the detection masks whose position and diameter can be freely chosen. Detection channels in the LiIO<sub>3</sub> case are positioned symmetrically on the opposite sides from the pump beam in noncritical phase-matching  $\varphi$  plane (Fig. 5.1 (a)), while in the BBO case, detection channels are localized in the directions where  $o$  and  $e$  parametric cones overlap (Fig. 5.1 (b)).

Single photons and photon coincidences are calculated using respectively (6.1)

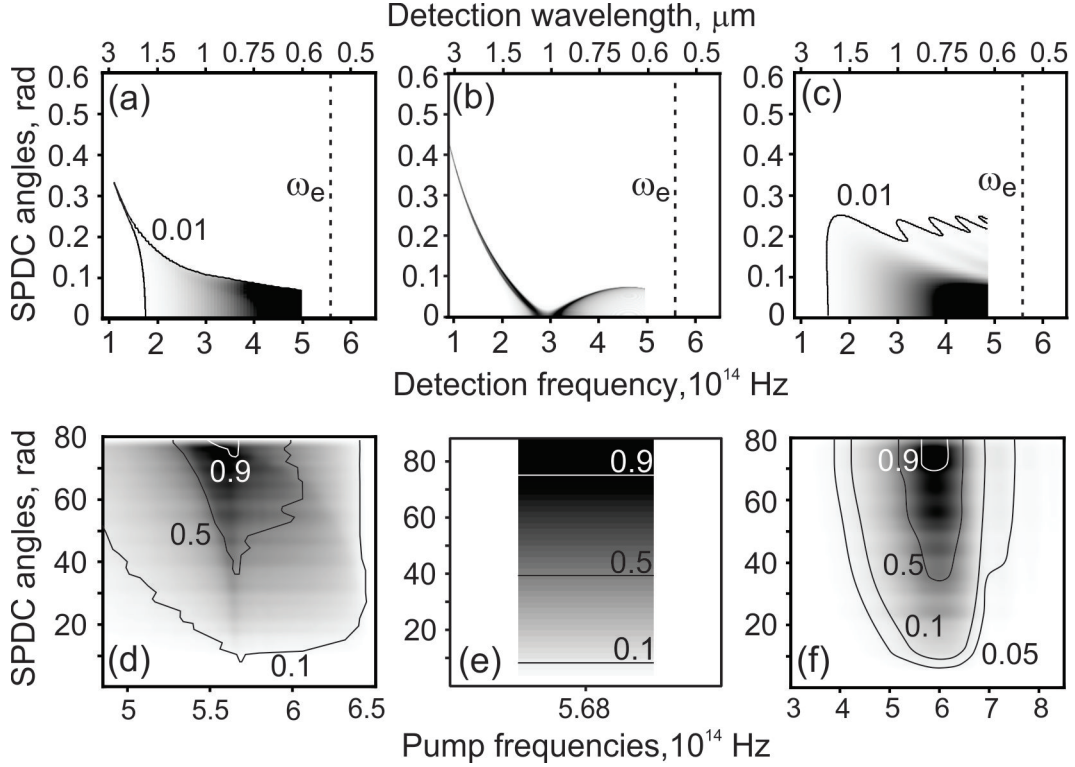


**Figure 6.2:** Frequency-angular distribution of biphoton density in detection band ((a - c)). Distribution of the aggregate biphoton field in pump spatial and frequency bands ((d - f)). Theoretical simulation was performed with the central frequency  $\omega_e = 5.68 \cdot 10^{14}$  Hz incoherent radiation exciting a 1 mm ((a), (d)) and 10  $\mu\text{m}$  ((c), (f)) length  $\text{LiNbO}_3$  crystal and with the monochromatic plane wave exciting a 1 mm length  $\text{LiNbO}_3$  crystal ((b), (e)). Contour lines with corresponding numbers are plotted with respect to the maximal value.

and (6.2) equations. It is considered that optical losses in the detection system do not exist. Simulation results (Fig. 6.3) reveal that a high (up to 70%) photon coincidence ratio can be expected in real experimental conditions. In the  $\text{LiIO}_3$  crystal case (Fig. 6.3 (a)), a photon coincidence ratio increase was observed in 5-50 nm spectral width range broadening the detection spatial spectrum (2-20 mrad), however, for broader detection the spatial spectra photon coincidence ratio started to decrease. The photon coincidence ratio becomes saturated for the broader detection spatial spectra. Small diameter apertures couple biphotons generated by the pump components from the relatively narrow space, therefore the photon coincidence ratio, which is determined by the ratio of effective pump spectral width to the detection spectral band, increases. In the BBO crystal case (Fig. 6.3 (b)), the photon coincidence ratio increases broadening detection spatial and frequency spectrum.

Simulation results show that incoherent sources can be used for high-quality biphoton field generation, equivalent to the quality of biphoton field excited by laser radiation. In order to maintain the high quality of photon coincidences, pump frequency spectrum must be narrower than the detection spectrum. When the pump spectral width is much narrower than the spectral width of the detection, the relative number of photon twins is mainly determined by the spectral width of the pump. Narrowing the pump spectrum to monochromatic radiation, the photon coincidence ratio approaches  $C = 1$  value, but the pump power approaches zero values.



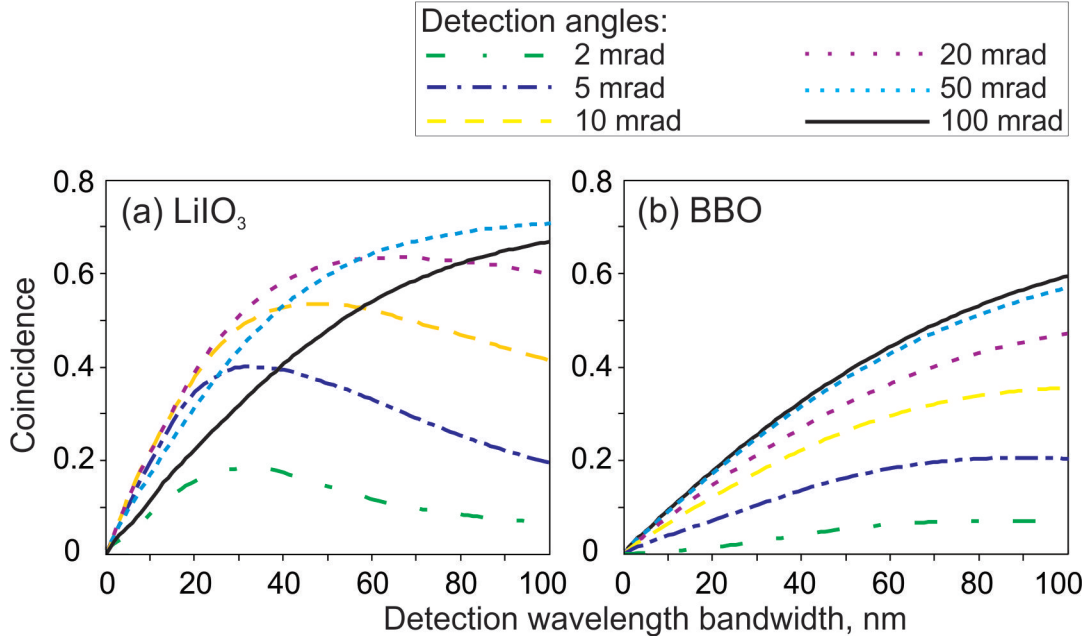


**Figure 6.3:** Photon coincidence probability dependence on the spatial and wavelength bandwidths of detection in type I  $\text{LiIO}_3$  (a) and type II BBO (b) crystals.

### 6.3 Theoretical simulation of experimental photon coincidence results

The theoretical model of biphoton field quality can now be used to analyze the experimental results discussed in chapter 5.3. Single photons are calculated using (6.1) and (6.4) formulas, photon coincidences - (6.2) and (6.5) formulas. In the theoretical model, factors are included such as the pump beam spatial dimensions, the pump beam walk-off in a nonlinear medium, the detection system transmittance, and so on. It is considered that the spatial range of the detector has a rectangular shape - all the waves that propagate within the numerical aperture of the fiber and the detection system spectral bandwidth are detected.

One of the most important experimental results - the single photon and photon coincidence dependence on the pump spatial spectral width and diameter. The simulation results qualitatively replicate the experimental values (Fig. 6.4). Single photons depend on the square of the pump spatial spectral width (Fig. 6.4 (a) the violet curve marks the values for the constant 0.8 mm pump diameter and different pump spatial spectral widths, the blue curve - constant 8 mm beam diameter), because pump power depends on the pump spatial spectral width by the same square law. The simulation also shows that single photon flux increases and becomes saturated with increasing pump beam diameter (Fig. 6.4 (a) the green curve corresponds to a constant 9 mrad pump spatial spectral width, the red curve - 40 mrad). Exactly the same tendencies regarding the pump spatial parameters are monitored in the photon coincidence simulation results (Fig. 6.4 (b)).

Comparing the simulation results with the experimental ones (Fig. 6.4,  $\times$  marks constant pump diameter,  $\square$  - spatial spectral width) it can be seen that these results qualitatively coincide. Small quantitative differences for the biggest pump beam diameter could be related to the incorrect evaluation of the geometric factor both for

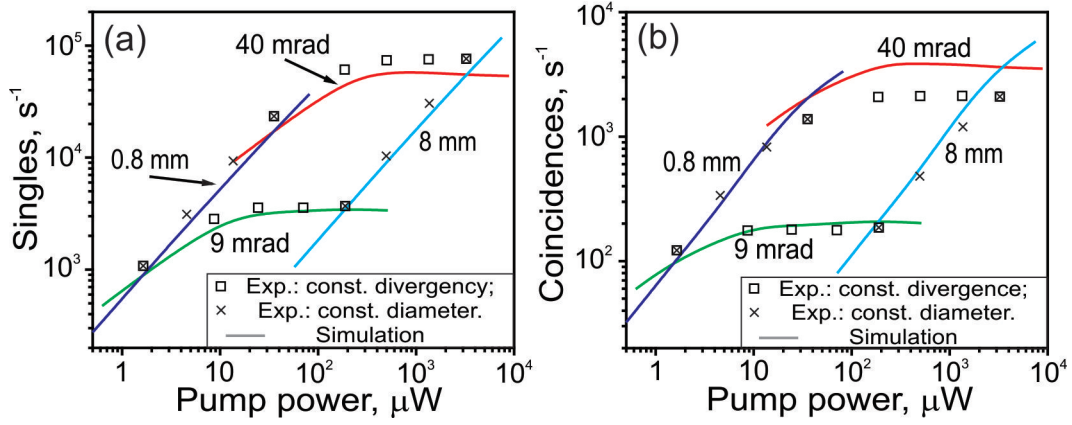


**Figure 6.4:** Single photons (a) and photon coincidence (b) flux dependence on the pump diameter and spatial spectrum. Experimental points correspond the values obtained using different pump spatial spectrum widths (9, 15, 25 or 40 mrad) and constant pump diameter ( $\times$ ) and using different pump diameter (0.8, 1.8, 3, 5 or 8 mm) and constant spatial spectral width ( $\square$ ). Solid lines correspond the theoretical simulation results obtained for the constant respective pump parameter.

single photons and photon coincidences due to the theoretical assumptions explained in chapter 6.1.1.

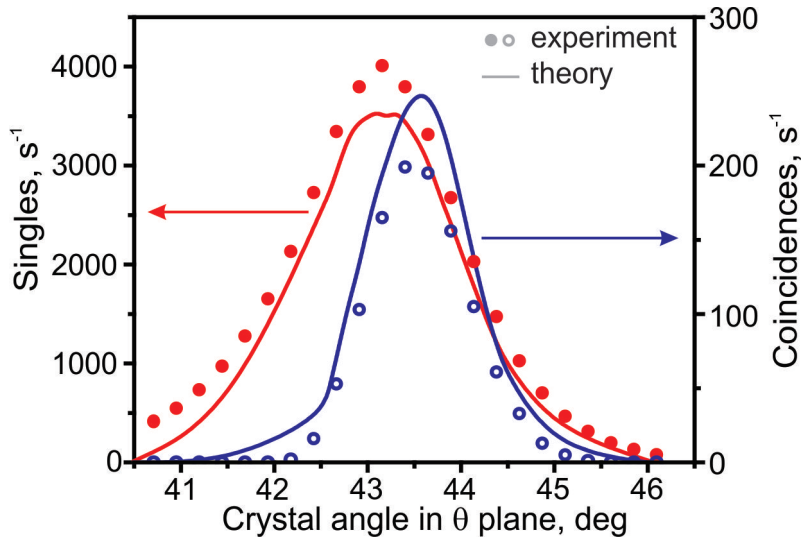


**Figure 6.5:** Single photons (red line and red rounds) and photon coincidences (blue line and blue circles) dependence on the  $\text{LiIO}_3$  crystal angle in  $\theta$  plane with respect to the pump beam. Solid lines – simulation results, circles and rounds – experimental results.

Detector spatial position influence on the photon coincidences was theoretically analyzed investigating the geometric factor changes displacing the detection areas in particular directions in respect to the crystal. The results of the theoretical simulation reproduce the experimental tendencies. Detection channels inclination in respect to the pump beam (Fig. 6.1) is realized in  $\varphi$  plane. Meanwhile, detection channels and pump beam in the  $\theta$  plane propagate in the same direction. Therefore, by displacing one detector in  $\theta$  plane, the detection volume directly travels out from the photon coincidence space and the photon coincidence ratio is determined by the core diameter of the fiber ( $105 \mu\text{m}$ ). In the meantime, by displacing a detector in  $\varphi$

plane, the detection volume also travels out from the photon coincidence space but at the same time photon coincidence volume travels to the beginning or to the end of the crystal. Due to the drift of the photon coincidence volume center along the length of the crystal, the function of the photon coincidence ratio dependence on the detectors position in  $\varphi$  plane is twice as wide as in  $\theta$  plane.

The simulation results for the single photon and photon coincidence flux dependence on crystal orientation are presented in Fig. 6.5. It can be seen that the theoretical results (solid curves) qualitatively coincide with the experimental results (circles and rounds). The quantitative difference between the results is related to the previously listed reasons - incorrect evaluation of the detection areas and positions, etc. Maximal theoretical values for both single photons and photon coincidences coincide with the experimental ones. Crystal orientation angles which correspond to the maximal values of both parameters differ by  $0.3^\circ$ . Also, the width of dependence functions is the same both for theoretical and experimental values. Thus, it can be concluded that changes of the parameters in respect to crystal angles are directly determined by the pump spatial and spectral properties and by the dispersion properties of the nonlinear medium.

## 6.4 Summary

In this chapter, a theoretical analysis was presented of biphoton field quality when exciting by incoherent radiation. The simulation of photon pair distribution in  $\text{LiNbO}_3$  crystal results show that it is possible to generate a biphoton field whose quality would be equivalent to the biphoton field excited by coherent sources. In order to create a high quality biphoton field, the pump frequency spectrum must be narrower than the detection frequency spectrum, whereas broadband pump frequency components, displaced far from the pump central frequency, could not create photon pairs in the detection spectral band. The simulation of photon coincidence experimental results in BBO and  $\text{LiIO}_3$  crystals showed that, with a real spectral features pump beam - blue LED, it is possible to generate sufficiently high photon coincidence ratios (up to 70%), depending on the spatial properties of detection. The theoretical model is well fitted to explain the experimental results.

# Conclusions

- First statement of defence is defended by this conclusion:
  1. For the first time, SPDC radiation was experimentally excited in type I KDP and  $\text{LiIO}_3$  and type II BBO crystals using  $0.5 \mu\text{W} - 0.53 \text{ mW}$  power broadband 457 nm central wavelength blue LED radiation as a pump source. It was determined that the power of SPDC excited by the incoherent radiation linearly depends on the pump power.
- Second statement of defence is defended by these conclusions:
  2. An SPDC theoretical simulation program was created that can simulate the spatial distribution of the SPDC excited by both spatially and temporally incoherent radiation. The program can be used to take into account such factors as the pump frequencies and spatial spectrum, the detection frequency range, nonlinear medium orientation with respect to the pump beam.
  3. It was determined that SPDC spatial distribution in various nonlinear crystals is determined by the individual dispersion characteristics of the media. The spatial characteristics of SPDC generated in type I KDP crystal are mainly determined by the pump beam spatial spectrum - increasing the pumping divergence, biphoton field asymmetry in the phase-matching  $\theta$  plane emerges. In smaller crystal angles side, the biphoton field is spatially more homogeneous and has higher spectral irradiance than in the bigger crystal angles side. Meanwhile, in the  $\text{LiIO}_3$  crystal case, the pump frequencies spectrum has the dominant influence – for the broader pump spectrum, the spread of the biphoton field increases.
- Third statement of defence is defended by these conclusions:
  4. For the first time, the biphoton field excited in  $\text{LiIO}_3$  crystal photon coincidence measurements were performed using  $1.64 \mu\text{W} - 3.26 \text{ mW}$  power broadband 404 nm central wavelength blue LED radiation as a pump source. Using the lowest pump power 1077 single photons/s and 122 coincidences/s fluxes were coupled into  $105 \mu\text{m}$  core diameter multimode fibers using 7 ns coincidence time window. As high as 11.5% photon coincidence ratio was recorded.
  5. It was determined that biphoton field pumped by the incoherent radiation single photon flux linearly depends on the pump power broadening spatial

pump distribution, while increasing the pump beam diameter the single photon flux significantly grows only for small diameter values (0.8 and 1.8 mm) and saturates increasing pump beam diameter. Photon coincidence flux duplicates characteristics of the single photon flux variation. The main differences are: the photon coincidence flux saturates more quickly with increasing the pump beam diameter, partial saturation of photon coincidence flux is observed also for the broadest pump spatial spectrum.

- Fourth statement of defence is defended by these conclusions:

6. The theoretical biphoton field excited by broadband incoherent radiation studies revealed that it is possible to achieve optimum conditions for qualitative and quantitative biphoton field generation with the proper selection of both the detection and the pump spectral properties. Modeling of spatial photon pairs distribution in the dispersing medium (LiNbO<sub>3</sub> crystal) showed that it is possible to create a biphoton field with an equivalent quality to the biphoton fields excited by coherent sources. Biphotons are located in a relatively narrow spatial area even with a very broad pump spatial spectrum. Theoretical modeling indicates that, in order to create a qualitative biphoton field the pump frequency spectrum must be narrower than the detection frequency spectrum.
7. It was determined that the photon coincidence ratio depends only on the broadband incoherent pump radiation frequencies spectrum and does not depend on pump spatial spectrum. On the other hand, the photon pairs flux is bigger when both frequency and spatial spectra are wider.

- Other conclusions:

8. A negative binomial distribution mode parameter was introduced which allows us to determine the avalanche photo detectors afterpulse generation probability performing statistical biphoton field analysis. Theoretical analysis showed that the distribution mode parameter is inversely proportional to the detectors afterpulse generation probability.
9. The biphoton field pumped by incoherent radiation photon coincidence ratio dependence on the detector position is bell-shaped. In the  $\theta$  plane, effective photon coincidence detection is limited by the fiber core - efficient detection area coincides with the fiber core diameter. Meanwhile, in the  $\varphi$  plane, the effective photon coincidence detection area is twice as broad. It was also found that the nonlinear medium orientation with respect to the pump beam is not critically important in the experimental conditions. Using the average parameters of the pump beam, effective photon coincidence detection is possible in quite a large range of crystal orientations. By tilting the crystal  $\pm 0.65^\circ$  from the angle corresponding to the maximum photon coincidence ratio value, this value does not decrease more than twice.
10. It was determined that the biphoton field is widely spread over many spatial modes performing the photon coincidence measurement with one single-mode and one multimode fiber. Single photon flux in a single-mode fiber

was as high as 17.5 photons/s, photon coincidence flux – 1.31 coincidences/s using 25 mrad and 5 mm diameter pump beam.

# Bibliography

- [1] R. W. Boyd, *Nonlinear Optics. Second Edition*, Academic Press, New York (2003).
- [2] W. H. Louisell and A. Yariv, Quantum fluctuations and noise in parametric processes. I, *Phys. Rev.*, **124**, 1646-1654 (1961).
- [3] J. P. Gordon, W. H. Louisell, and L. R. Walker, Quantum fluctuations and noise in parametric processes. II, *Phys. Rev.*, **129**, 481-485 (1963).
- [4] S. E. Harris, M. K. Oshman, and R. L. Byer, Observation of tunable optical parametric fluorescence, *Phys. Rev. Lett.*, **18**, 732–734 (1967).
- [5] R. L. Byer and S. E. Harris, Power and bandwidth of spontaneous parametric emission, *Phys. Rev.*, **168**, 1064-1068 (1968).
- [6] B. E. A. Saleh, B. M. Jost, H. B. Fei, and M. C. Teich, Entangled-photon virtual-state spectroscopy, *Phys. Rev. Lett.*, **80**, 3483–3486 (1998).
- [7] T. Jennewein, C. Simon, G. Weihs, H. Weinfurter, and A. Zeilinger, Quantum cryptography with entangled photons, *Phys. Rev. Lett.*, **84**, 4729–4732 (2000).
- [8] A. N. Boto, P. Kok, D. S. Abrams, S. L. Braunstein, C. P. Williams, and J. P. Dowling, Quantum interferometric optical lithography: exploiting entanglement to beat the diffraction limit, *Phys. Rev. Lett.*, **85**, 2733–2736 (2000).
- [9] K. C. Toussaint, G. Di Giuseppe, K. J. Bycenski, A. V. Sergienko, B. E. A. Saleh, and M. C. Teich, Quantum ellipsometry using correlated-photon beams, *Phys. Rev. A*, **70**, 023801(1-7) (2004).
- [10] R. Thew and N. Gisin, Quantum communication, *Nat. Photon.*, **1**, 165-171 (2007).
- [11] I. P. Degiovanni, M. Genovese, V. Schettini, M. Bondani, A. Andreoni, and M. G. A. Paris, Monitoring the quantum-classical transition in thermally seeded parametric down-conversion by intensity measurements, *Phys. Rev. A*, **79**, 063836(1-7) (2009).
- [12] P. M. Anisimov, G. M. Raterman, A. Chiruvelli, W. N. Plick, S. D. Huver, H. Lee, and J. P. Dowling, Quantum metrology with two-mode squeezed vacuum: parity detection beats the Heisenberg limit, *Phys. Rev. Lett.*, **104**, 103602(1-4) (2010).

- [13] P. G. Kwiat, K. Mattle, H. Weinfurter, and A. Zeilinger, New high-intensity source of polarization-entangled photon pairs, *Phys. Rev. Lett.*, **75**, 4337–4341 (1995).
- [14] D. C. Burnham and D. L. Weinberg, Observation of simultaneity in parametric production of optical photon pairs, *Phys. Rev. Lett.*, **25**, 84–87 (1970).
- [15] D. L. Weinberg, Observation of optical parametric noise pumped by a mercury lamp, *J. Appl. Phys.*, **41** 4239 (1970).
- [16] D. N. Klyshko, *Photons and Nonlinear Optics*, Gordon and Breach Science Publishers (1988).
- [17] Y. R. Shen, *The Principles of Nonlinear Optics*, John Wiley & Sons, New York (1984).
- [18] D. Magde and H. Mahr, Study in ammonium dihydrogen phosphate of spontaneous parametric interaction tunable from 4400 to 16 000 Å, *Phys. Rev. Lett.*, **18**, 905–907 (1967).
- [19] V. M. Petnikova, Nonlinear optical efficiency of two-photon fields, *Sov. J. Quantum Electron.*, **9**, 276-280 (1979).
- [20] J. G. Rarity, K. D. Ridley, and P. R. Tapster, Absolute measurement of detector quantum efficiency using parametric downconversion, *Appl. Opt.*, **26**, 4616–4619 (1987).
- [21] E. C. Cheung, K. Koch, G. T. Moore, and J. M. Liu, Measurements of second-order nonlinear optical coefficients from the spectral brightness of parametric fluorescence, *Opt. Lett.*, **19**, 168–170 (1994).
- [22] G. Borsa, S. Castelletto, A. Godone, C. Novero, and M. L. Rastello, Measurement of second-order optical nonlinear coefficient from the absolute radiant power of parametric fluorescence in  $\text{LiIO}_3$ , *Optical Review*, **4**, 484-489 (1997).
- [23] F. A. Ponce, and D. P. Bour, Nitride-based semiconductors for blue and green light-emitting devices, *Nature*, **386**, 351–359 (1997).
- [24] D. N. Nikogosyan, *Nonlinear Optical Crystals: A Complete Survey*, Springer Science+Business Media, Inc, New York (2005).
- [25] W. P. Grice and I. A. Walmsley, Spectral information and distinguishability in type-II down-conversion with a broadband pump, *Phys. Rev. A*, **56**, 1627-1634 (1997).
- [26] P. S. K. Lee, M. P. van Exter, and J. P. Woerdman, How focused pumping affects type-II spontaneous parametric down-conversion, *Phys. Rev. A*, **72**, 033803(1-5) (2005).
- [27] F. T. Arecchi, Measurement of the statistical distribution of Gaussian and laser sources, *Phys. Rev. Lett.*, **15**, 912-916 (1965).



- [28] C. Walck, *Hand-book on Statistical Distributions for experimentalists*, University of Stockholm (2007).
- [29] F. Träger, *Springer Handbook of Lasers and Optics*, New York N.Y.: Springer, 3-32 (2007).
- [30] J. W. Goodman, *Statistical Optics*, John Wiley & Sons, Inc., New York, 465–490 (2000).
- [31] L. Mandel and E. Wolf, *Optical Coherence and Quantum Optics*, Cambridge University Press, New York (1995).
- [32] W. Wasilewski, C. Radzewicz, R. Frankowski, and K. Banaszek, Statistics of multiphoton events in spontaneous parametric down-conversion, *Phys. Rev. A*, **78**, 033831(1-8) (2008).
- [33] M. Avenhaus, H. B. Coldenstrodt-Ronge, K. Laiho, W. Mauerer, I. A. Walmsley, and C. Silberhorn, Photon number statistics of multimode parametric down-conversion, *Phys. Rev. Lett.*, **101**, 053601(1-4) (2008).
- [34] J. Peřina Jr., O. Haderka, and V. Michálek, Sub-Poissonian-light generation by postselection from twin beams, *Optics Express*, **21**, 19387-19394 (2013).
- [35] M. Lamperti, A. Allevi, M. Bondani, R. Machulka, V. Michálek, O. Haderka, and J. Peřina, Jr., Optimal sub-Poissonian light generation from twin beams by photon-number resolving detectors, *J. Opt. Soc. Am. B*, **31**, 20-25 (2014).
- [36] L. Campbell, Afterpulse measurement and correction, *Rev. Sci. Instrum.*, **63**, 5794-5798 (1992).
- [37] G. F. Zhang, S. L. Dong, T. Huang, Y. Liu, J. Wang, L. T. Xiao, and S. T. Jia, Photon statistical measurement of afterpulse probability, *Int. J. Mod. Phys. B*, **22**, 1840–1845 (2008).
- [38] C. K. Hong, Z. Y. Ou, and L. Mandel, Measurement of subpicosecond time intervals between two photons by interference, *Phys. Rev. Lett.*, **59**, 2044-2046 (1987).
- [39] C. Liang, K. F. Lee, M. Medic, P. Kumar, R. H. Hadfield, and S. W. Nam, Characterization of fiber-generated entangled photon pairs with superconducting single-photon detectors, *Optics Express*, **15**, 1322-1327 (2007).
- [40] Y. H. Kim, Two-Photon Interference without bunching two photons, *Physics Letters A*, **315**, 352–357 (2003).
- [41] C. Eckart and F. R. Shonka, Accidental coincidences in counter circuits, *Phys. Rev.*, **53**, 752-756 (1938).

## Santrauka

# PARAMETRINĖS FLUORESCENCIJOS ŽADINAMOS NEKOHERETINIAIS ŠVIESOS ŠALTINIAIS TYRIMAS

Parametrinė fluorescencija – nekoherentinė šviesos sklaida – yra vienas pagrindinių susietųjų fotonų šaltinių taikomų kvantinės optikos eksperimentuose. Nuo pat pirmųjų parametrinės fluorescencijos eksperimentinių tyrimų 1968 metais įsigalėjo tradicija šį reiškinį žadinti išimtinai lazerine spinduliuote.

Šios disertacijos tikslas – eksperimentiškai ištirti galimybę generuoti parametrinę fluorescenciją tiek laikiškai, tiek ir erdviškai nekoherentine spinduliuote – didelės galios šviesos diodu. Taip pat nustatyti, kokią įtaką turi erdvinė ir spektrinė kaupinimo spinduliuotės sudėtis dvyninio lauko savybėms, nustatyti galimybes keisti dvyninio lauko struktūrą, išnagrinėti galimybes dvyninį lauką, žadinamą mėlynu šviesos diodu, taikyti kvantinės optikos eksperimentuose.

Atliekant tyrimus didelio jautrio CCD kamera buvo registruojami silpni parametrinės fluorescencijos signalai, pavienių fotonų skaitliukais buvo registruojami fotonų sutapimai, kurie yra vienas pagrindinių parametrų, kuriuo charakterizuojami susietųjų fotonų šaltiniai kvantinės optikos eksperimentuose. Lygiagrečiai eksperimentiniams tyrimams buvo atliekami teoriniai skaičiavimai. Šiuo tikslu buvo parašytas matematinio modeliavimo programinis kodas, skirtas įvertinti parametrinės fluorescencijos erdvinį galios pasiskirstymą bei modeliuoti fotonų sutapimų eksperimentą, keičiant kaupinimo pluošto tiek erdvines, tiek ir spektrines savybes, keičiant detekcijos sistemos erdvines ir spektrines savybes.

Šio darbo rezultatai atskleidžia, kad nekoherentiniai šaltiniai gali būti puiki alternatyva lazerinėms sistemoms siekiant žadinti vidutinės kokybės dvyninius laukus, ypač tokiose tyrimų srityse, kuriose mažas dvyninio lauko koherentiškumas būtų didžiulis privalumas. Pagrindiniai nekoherentinių šaltinių pranašumai prieš lazerines sistemas: maža kaina, paprasta gamybos technologija ir didžiulė komercinė skirtingo bangos ilgio šaltinių įvairovė.

# Curriculum vitae

## JUSTINAS GALINIS

Date of birth: 1986 November 7

Place of birth: Elektrėnai, Lithuania

Nationality: Lithuanian

### Education:

1992 – 2004 Elektrėnai gymnasium (high school)  
1994 – 2002 Elektrėnai music school  
2004 – 2008 Vilnius University - Physics (Bachelor)  
2008 – 2010 Vilnius University - Laser Physics and Optical Technologies (Master)

### Work Experience:

2006 – 2010, 2013	Department of Quantum Electronics, Vilnius University	technician, young researcher
2007 11	Science and art exhibition “Light in Light”	guide
2008 – 2010	Institute of science and encyclopedia publishing	scientific editor
2008 – 2010	Vilnius College, Health care faculty	assistant
From 2011	General Physics Practice Laboratory, Department of Quantum Electronics, Vilnius University	engineer, technician, lecturer

### Summer schools:

- STELLA school 2011, „School for Training in Experiments with Lasers and Laser Applications“, 20th June – 8th July, 2011, University of Insubria, Como (Italy)
- The 20th Jyväskylä Summer School, 9th – 20st August 2010, University of Jyväskylä (Finland)
- OLA (Optoelectronics, Lasers and Applications) Summer School 2008, June 30 – July 11, Electronics Department of the Technological Educational Institute of Crete, Chania

### Internships:

- In 2012 interned for 3 months in Insubria University (Como, Italy)
- In 2013 interned for 1 month in Joint Laboratory of Optics (Olomouc, Czech Republic)

### Other information:

- 2004 – 2011 sang in Vilnius University mixed voices chorus "Gaudeamus".
- From 2011 sings in chamber chorus "Aidija".